lee 07-03-03A08:41 RCVD

# REPORT DOCUMENTATION PAGE

AFRL-SR-AR-TR-03-

03365

Public reporting burden for this collection of information is estimated to average 1 hour per response, including the time for reviewing data needed, and completing and reviewing this collection of information. Send comments regarding this burden estimate or any oth this burden to Department of Defense, Washington Headquarters Services, Directorate for Information Operations and Reports (070 4302. Respondents should be aware that notwithstanding any other provision of law, no person shall be subject to any penalty for f valid OMB control number. **PLEASE DO NOT RETURN YOUR FORM TO THE ABOVE ADDRESS.**

ng the lucing 202- urrently

**1. REPORT DATE** *(DD-MM-YYYY)*
01/06/2003

**2. REPORT TYPE**
Final Report

**3. DATES COVERED** *(From - To)*
From 14/04/1999 to 14/10/2002

**4. TITLE AND SUBTITLE**
Micro-stress and Failure Analysis of Textile Composites

**5a. CONTRACT NUMBER**
F49620-99-1-0240

**5b. GRANT NUMBER**
F49620-99-1-0240

**5c. PROGRAM ELEMENT NUMBER**

**5d. PROJECT NUMBER**

**5e. TASK NUMBER**

**5f. WORK UNIT NUMBER**

**6. AUTHOR(S)**
Youqi Wang
Department of Mechanical and Nuclear Engineering
Kansas State University
Manhattan, KS 66506

**7. PERFORMING ORGANIZATION NAME(S) AND ADDRESS(ES)**
Kansas State University 2 Fairchild Hall
Manhattan, KS 66506-1103

**8. PERFORMING ORGANIZATION REPORT NUMBER**

**9. SPONSORING / MONITORING AGENCY NAME(S) AND ADDRESS(ES)**
Air Force Office of Scientific Research
801 N. Randolph St., Rm. 732
Arlington, VA 22203-1977

**10. SPONSOR/MONITOR'S ACRONYM(S)**
AFOSR

**11. SPONSOR/MONITOR'S REPORT NUMBER(S)**

**12. DISTRIBUTION / AVAILABILITY STATEMENT**
Approved for public release;
distribution unlimited.

20031028 212

**13. SUPPLEMENTARY NOTES**

**14. ABSTRACT**

Project objectives are the development of more optimal mechanics approaches for textile composite design and failure analysis. Tailoring of the textile composite microstructure is one of the most pressing research issues in textile composite design. The textile pre-forming process determines the microstructure of the textile preform. Preform microstructure determines textile composite micro-stress distribution. Development of a numerical approach that facilitates establishment of relations between textile microstructures and textile processes is, therefore, critical. In this project, two new numerical methods are developed. The first is a digital element simulation approach for textile mechanics. It enables simulation of the textile process as well as simulation of textile preform deformation. As a result, detailed knowledge of the textile preform microstructure becomes obtainable. The second method developed in this project is a heterogeneous element method for the micro-stress analysis of textile composites. Formulation of a heterogeneous element guarantees that both the equilibrium conditions and the continuity of displacement at the interface are satisfied. Yet, it allows for interface stress and strain jump. Because the formulation reflects the actual physical situation at the interface, it provides a much more accurate result than conventional approaches if the same mesh is used.

**15. SUBJECT TERMS**

| 16. SECURITY CLASSIFICATION OF: None | | | 17. LIMITATION OF ABSTRACT | 18. NUMBER OF PAGES | 19a. NAME OF RESPONSIBLE PERSON |
|---|---|---|---|---|---|
| a. REPORT | b. ABSTRACT | c. THIS PAGE | | 40 | Youqi Wang |
| | | | | | 19b. TELEPHONE NUMBER *(include area code)* 785-532-7181 |

**Standard Form 298 (Rev. 8-98)**
**Prescribed by ANSI Std. Z39.18**

# MICRO-STRESS AND FAILURE ANALYSIS OF TEXTILE COMPOSITES

## Final Report

**Principal Investigator:** Youqi Wang
Department of Mechanical and Nuclear Engineering
302 Rathbone Hall
Kansas State University,
Manhattan, KS 66506
Tel: 785-532-7181,
E-mail: wang@mne.ksu.edu

**Institution:** Kansas State University
2 Fairchild Hall
Manhattan, KS 66506-1103

**Grant Number:** **F49620-99-1-0240**

**Period of Performance:** **April 15, 1999 - October14, 2002**

# MICRO-STRESS AND FAILURE ANALYSIS OF TEXTILE COMPOSITES

*Youqi Wang*
*Department of Mechanical and Nuclear Engineering*
*Kansas State University*
*Manhattan, KS 66506*
*Final Report*

## I. OBJECTIVES

Project objectives are the development of more optimal mechanics approaches for textile composite design and failure analysis. Tailoring of the textile composite microstructure is one of the most pressing research issues in textile composite design. The textile pre-forming process determines the microstructure of the textile preform. Preform microstructure determines textile composite micro-stress distribution. Development of a numerical approach that facilitates establishment of relations between textile microstructures and textile processes is, therefore, critical. In this project, two new numerical methods are developed. The first is a digital element simulation approach for textile mechanics. It enables simulation of the textile process as well as simulation of textile preform deformation. As a result, detailed knowledge of the textile preform microstructure becomes obtainable. The second method developed in this project is a heterogeneous element method for the micro-stress analysis of textile composites. Formulation of a heterogeneous element guarantees that both the equilibrium conditions and the continuity of displacement at the interface are satisfied. It also allows for interface stress and strain jump. Because the formulation reflects the actual physical situation at the interface, it provides a much more accurate result than conventional approaches given the use of the same mesh. This project serves the interest of the Air Force Research Laboratory because it contributes to the goal of its on-going project "Micro-mechanical Failure Criteria." The contact persons at the Air Force Research Laboratory are Senior Scientists, Dr. Nick Pagano and Dr. Ajit Roy.

## II. DIGITAL ELEMENT ANALYSIS IN TEXTILE MECHANICS

### 2.1 Basic Concept of Digital Element Analysis

Digital element analysis is a new numerical tool developed in this project for textile mechanics. It can be used for textile process design and fabric deformation, strength and failure analysis. In digital element analysis, each fiber or yarn is modeled as a frictionless pin-connected rod element chain. These rod elements are defined as "digital elements." Contacts between fibers or yarns are modeled by contact elements. Textile processes and fabric deformation are formulated as a non-continuum mechanics problem with boundary conditions. A procedure, similar to finite element analysis, is adopted to derive yarn movement during textile processes or fabric deformation.

Three critical concepts suffuse digital element analysis: digital chain, contact between digital chains, and yarn assembly.

2.1.1 Digital chain

A digital chain is composed of many rod-elements, defined as "digital elements", as shown in Fig.1. Frictionless pins, defined as "nodes", connect rod-elements. As the length of these rod-elements approaches zero, the digital chain becomes fully flexible. It is thus able to represent a one-dimensional flexible physical entity with a fixed cross-section, such as fibers and yarns.

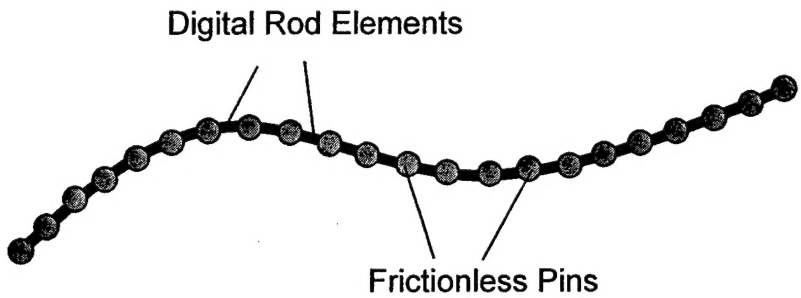


Fig.1 Concept of Digital Chain

In digital element simulation, the flexible nature of a digital chain is conveyed by frictionless-pins, which connect digital elements. Digital element size must be very small. Otherwise, physicality (in this case, flexibility) cannot be preserved. The digital chain is a digital representation of a flexible physical entity. Digital element length reflects digital discretization resolution.

The stiffness matrix of the digital element is the same as the stiffness matrix of the rod element used in finite element analysis [1-2], which can be expressed as:

$$[K]=\frac{EA}{L}\begin{bmatrix} 1 & 0 & 0 & -1 & 0 & 0 \\ 0 & \Delta & 0 & 0 & -\Delta & 0 \\ 0 & 0 & \Delta & 0 & 0 & -\Delta \\ -1 & 0 & 0 & 1 & 0 & 0 \\ 0 & -\Delta & 0 & 0 & \Delta & 0 \\ 0 & 0 & -\Delta & 0 & 0 & \Delta \end{bmatrix} \tag{1}$$

where $E$ is the modulus, $A$ is the cross-section area, $L$ is the length of the digital element and $\Delta$ is a small perturbation used to prevent the singularity of the global stiffness matrix. $\Delta$ must be much smaller than 1. Generally speaking, it is on the order of $10^{-6} - 10^{-12}$.

2.1. 2 Contacts between Digital Chains

When the element length approaches zero, contact between two digital chains can be represented by contact between nodes from two neighboring chains. See Fig.2. If the distance between two nodes is smaller than the diameter of the digital chain, a contact element is added between them. The stiffness matrix can be expressed as

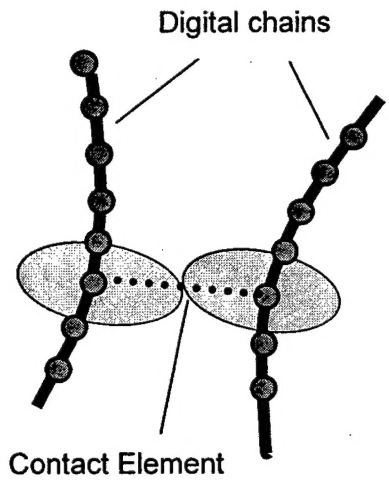


Fig.2 Contact Element between Two Neighboring Digital Chains

$$\begin{bmatrix} k_n & 0 & 0 & -k_n & 0 & 0 \\ 0 & -k_s & 0 & 0 & +k_s & 0 \\ 0 & 0 & -k_s & 0 & 0 & +k_s \\ -k_n & 0 & 0 & k_n & 0 & 0 \\ 0 & +k_s & 0 & 0 & -k_s & 0 \\ 0 & 0 & +k_s & 0 & 0 & -k_s \end{bmatrix} \tag{2}$$

where $k_n$ and $k_s$ are the compression stiffness coefficient and the lateral stiffness coefficient, respectively.

If contact occurs between two nodes, one of two kinds of physical conditions would exist: sticking or sliding.

Two digital chains would stick together if $\mu F_n > |F_s|$, where $\mu$ is the friction coefficient, $F_n$ is the compressive force between two nodes, and $F_s$ is shear force between two digital chains. In a rigid contact, displacements of node $i$ and node $j$ are constrained to be the same. Thus, the penalty method can be employed. Stiffness coefficients $k_n$ and $k_s$ are replaced by a large penalty number.

Sliding occurs between two yarns if $\mu F_n \leq |F_s|$. If this occurs, the lateral stiffness coefficient $k_s$ would be zero.

2.1.3 Yarn Assembly

Two digital element analysis models have been developed. One is called "single chain digital element analysis"; the other is called "multi-chain digital element analysis". The former operates on the level of yarn; the latter on the level of fiber.

Single-chain digital element analysis

In a single chain digital element analysis, a yarn is modeled as a single digital chain. It is a flexible, one-dimensional physical entity with a constant cross-section, most commonly circular. Once the yarn is discretized into digital element chains, each element receives an element number and each node receives a nodal number. Then, contact elements are positioned between two neighboring digital chains if they contact each other. The element stiffness matrices are calculated and a global stiffness matrix is assembled. Given specific boundary conditions, nodal displacements and element stress and strain can be derived. Yarn paths inside a fabric are defined by nodal positions; yarn tensions are defined by element stresses.

Fig.3 shows a simple twisting process simulated by single chain digital element analysis. Fig.3-a is the set-up for the twisting process. Two spring elements are placed at the bottom of the yarns in order to maintain yarn tension. First, the top ends of the two yarns are moved upward a distance of $\Delta h$ to achieve initial yarn tension. This provides a pre-twist yarn tension. Then, the bottom ends of both spring elements rotate along a circular tract. Thus, a twisted yarn is produced. Fig.3-b is the twisted yarn created by digital element simulation. One also can visualize the length of the digital elements from 3-b.

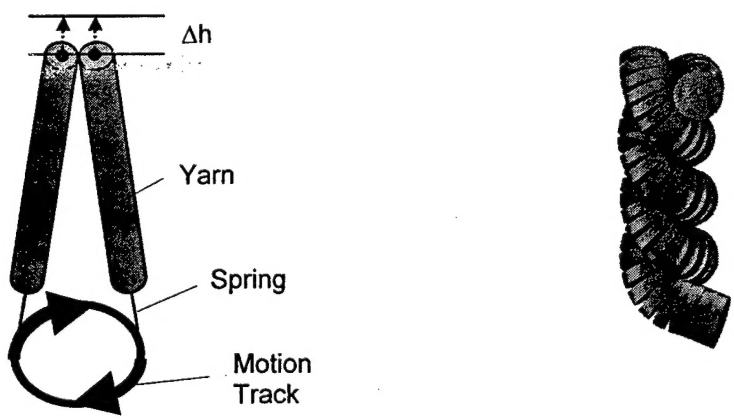


3-a Numerical Model 3-b Twisted Yarn

Fig.3 Digital Model and Simulation Results for the Twisting Process

Multi-chain digital element analysis

Multi-chain digital element analysis follows physicality more precisely. In this model, each fiber is modeled as a digital chain and each yarn is composed of many fibers, i.e. a yarn is modeled as an assembly of digital chains. After fibers are discretized into digital chains and after yarn is assembled, the process used in the previous model can be adopted. Fiber paths are defined by nodal positions. Yarn is defined as an assembly of fibers. Fiber tension and strain are defined by element stress and strain. Yarn tension is the summation of fiber tensions within the yarn. Yarn cross-section shape is defined by fiber arrangement within the yarn. The method can be used to simulate textile processes and fabric deformation under both static and dynamic loads. Compared to the single chain digital element approach, the multi-chain model can much more accurately derive both yarn movement and cross-section deformation. Yarn cross-section deformation influences yarn paths during forming and deformation processes. Both yarn and fiber tension can thus be predicted. This allows investigation of fabric failure mechanisms under external loads.

During the textile process, inter-fiber compression and friction play important roles in fabric deformation and failure. Because the multi-chain digital element approach closely follows physicality, it should provide a much more accurate result than the single chain digital element analysis for the prediction of fabric micro-geometry, deformation and strength.

Physically, a yarn is composed of hundreds or thousands of fibers. Current computer power limits the amount of chains that can be used to model each yarn. In most cases, 19-50 digital chains are sufficient to represent yarn cross-section geometry.

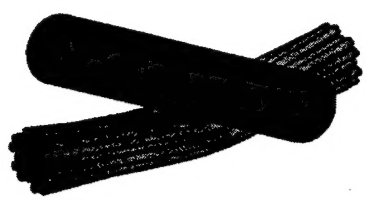

4-a Yarn under Single Side Compression

4-b Deformed Yarn

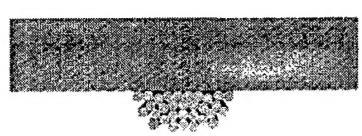

4-c Middle Cross Section

Fig.4 Yarn Deformation under Single Side Compression

Fig.4 illustrates the simplest example of multi-chain digital element analysis. A yarn is under single side compression. It is modeled as an assembly of 32 digital chains. Fig.4-a shows the loading condition. Fig.4-b is an isometric view of the deformed yarn. Fig.4-c is the middle cross-section shape of the deformed yarn.

## 2.2 Numerical Examples

Two numerical examples are presented in this section. In the first example, a two-dimensional weaving process is simulated using both single- and multi- chain models. In the second example, a three-dimensional braiding process is simulated. One can compare the difference between the microstructures calculated by use of the two different approaches.

### 2.2.1 Two-Dimensional Weaving Process

A two-dimensional weaving process was simulated using the single chain digital element approach. A step-by-step simulation of the weaving process is illustrated in Fig.5. Tensions applied to wefts and warps are the same through out the process. Fig.6 is a woven fabric generated by the single chain digital element model. Although yarns are compressed from the top or the bottom during the weaving process, this model cannot simulate yarn cross-section deformation, as shown in the figure 6.

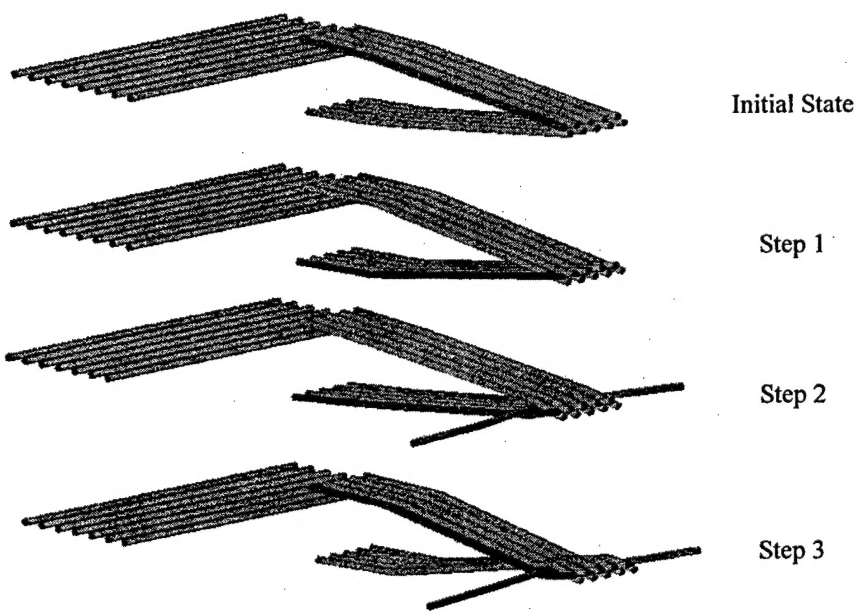


Fig.5 Step-by-Step Simulation of the 2-D Weaving Process

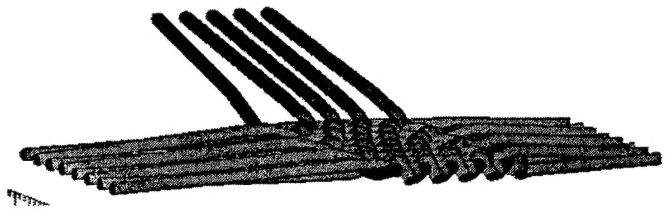

Fig.6 2-D Woven Fabric Generated by Single Chain Digital Element Model

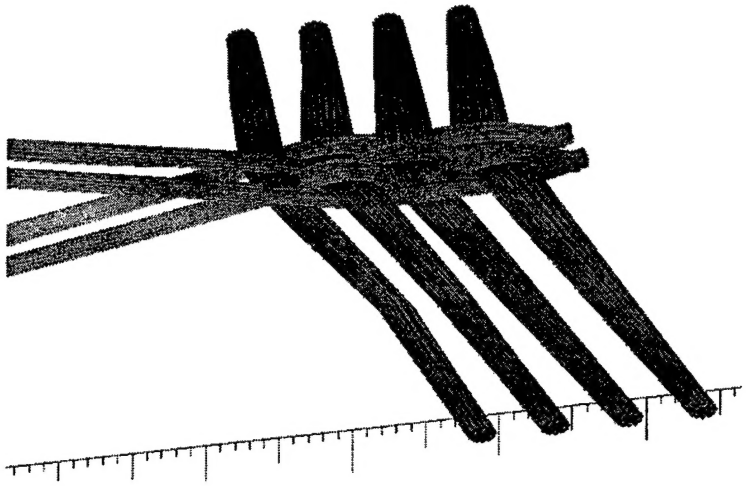

Fig.7 2-D Woven Fabric Generated by Multi-Chain Digital Element Model

Fig.7 displays a woven fabric generated using the multi-chain digital element model with the same weaving process. Each yarn is an assembly of 19 digital chains. Total cross-section area of the 19 fibers is equal to the cross section area of the single yarn. Other parameters taken in the simulation are the same. Fig.8 illustrates yarn cross-section along different sections inside the fabric. Fig.8-a is the cross-section along the warp direction. Fig.8-b is the five cross-sections along the weft direction. The positions of the five cross-sections are defined in Fig.8-a. For the sake of clarity, cross-sections of fibers that belong to the same yarn have the same color. Although only 19 fibers are used for each yarn, one can observe that yarn cross-section varies from one position to another.

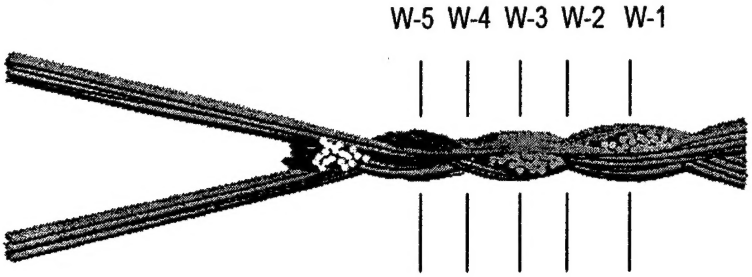


8-a Side View along Warp Direction

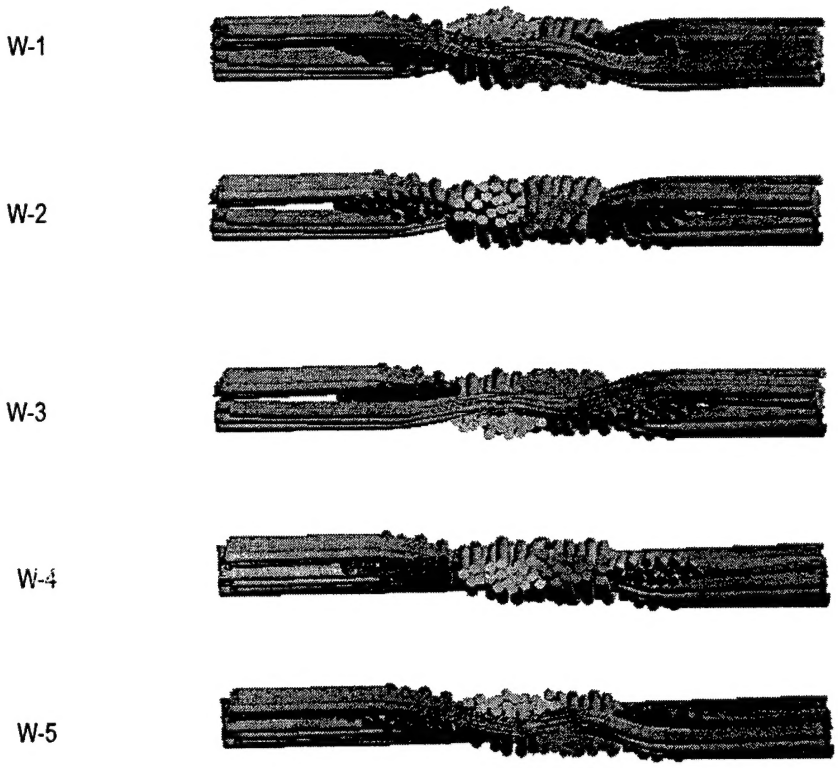


8-b Cross-Sections along the Weft Direction

Fig.8 Cross-Sections of 2-D Woven Fabric Generated by Multi-Chain Digital Element Model

2.2.2. Three-Dimensional Braiding Process

The microstructure of the three-dimensional braided preform is much more complex than the conventional two-dimensional textile preform. Yarn topology and geometry inside a preform cannot be observed from the surface of the fabric. Because yarns are entangled and because yarn axes inside most textile preforms extend as a three-dimensional spatial curve, it is very difficult to investigate detailed yarn geometry even with the use of a microscope.

Fig.9-a is a three-dimensional braided preform generated by use of the single chain digital element model. Fig.9-b is the cross-section of the preform. Fig.10-a shows a three-dimensional braided preform generated by use of the multi-chain digital element model. Fig.10-b is the cross-section of the preform. Although these two preforms have the same topology, their respective micro-geometries differ. Fig.10-c is the isometric view of the multi-chain preform. Yarn cross-section shapes vary from section to section. Cross-section deformation, in tern, affects the spatial paths of yarns and the volume fraction of fibers. Both the spatial paths of yarns and the volume fraction of fibers play critical roles in the determination of the mechanical properties and failure mechanisms of textile composites.

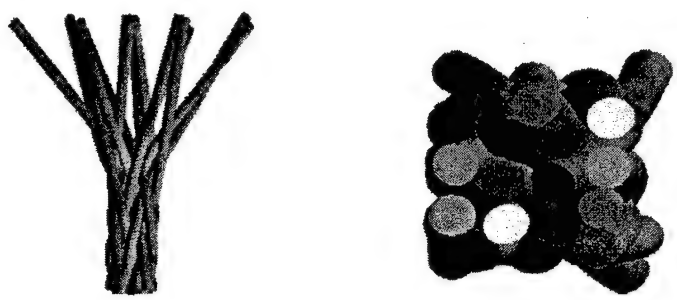

9-a 3-D Braided Preform 9-b Preform Cross-Section

Fig.9 3-D Braided Preform Generated by the Single Chain Digital Element Model

2.3 Conclusions

In this project, digital element analysis is used to simulate textile processes. Yet the value of the approach is much more extensive. It is a general numerical approach: it can be used to investigate other mechanics problems, such as the deformation of textile preforms during the manufacturing process of textile composites. Further, it enables calculation of fiber tension inside fabrics. As such, it also can be employed to investigate the strength and failure mechanisms of textile fabrics under both static and dynamic loads. Given specific boundary conditions and specific external loads, the digital element model can also be used to simulate the failure process step by step and to predict the strength of the fabric.

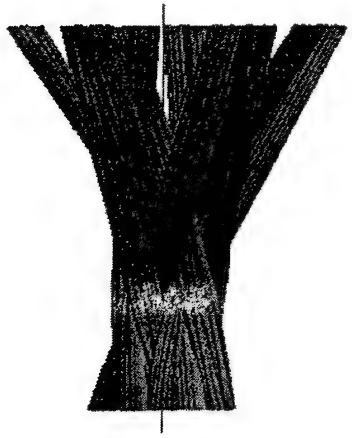

10-a 3-D Braided Preform

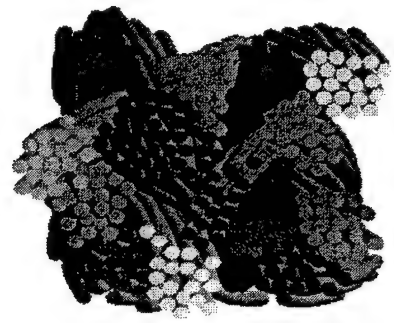

10-b Cross-Section

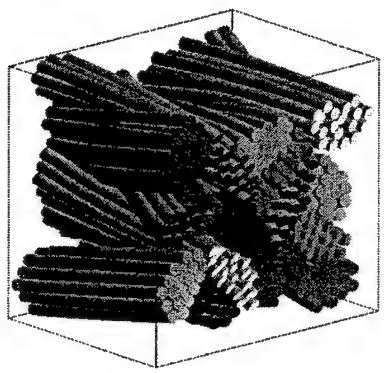

10-c Isometric View

Fig.10 3-D Braided Preforms Generated by Multi-Chain Digital Element Models

## III. HETEROGENEOUS FINITE ELEMENT ANALYSIS

### 3.1 Introduction

Micro-failure often emanates from the yarn (fiber)-matrix interface. It can be caused by interfacial stress concentration or interfacial debond. Therefore, it is important to predict interfacial stress concentration. Many attempts have been undertaken using the conventional finite element approach. However, there have been two great obstacles:

1. The modulus of the fibers (or yarns) can be 50-100 times higher than the matrix. Serious stress concentration along the yarn-matrix and fiber-matrix interfaces therefore exists. It is important to predict this interfacial stress concentration. Use of the conventional iso-

parametrical displacement element cannot satisfy the equilibrium conditions along the interface. It thus provides poor prediction performance of interfacial stress concentration. Significant error may occur even with employment of a fine mesh. A commonly considered way to improve the convergent rate of stress is to employ a mixed or hybrid finite element method, as it is possible to construct compatible stress functions. However, due to the huge difference of moduli between fibers and matrix, there is a tangential stress jump at the interface between the two materials. Even with the employment of a compatible stress function, the element still fails to model the stress jump, so it still may be unable to converge to the actual stress at the interface.

2. It is very difficult to match element boundaries to the yarn-matrix and fiber matrix interfaces because textile composite microstructure is very complex.. The micro-geometry of the yarn cross section varies from cross-section to cross-section, so mesh generation is a time consuming and tedious task.

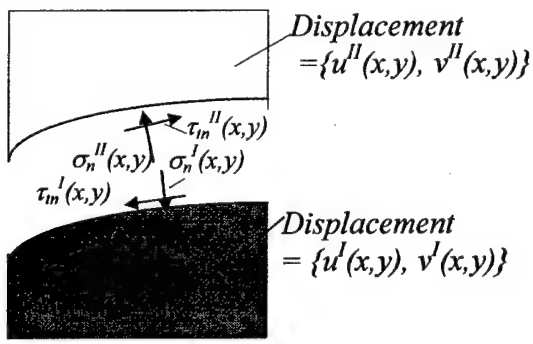


Fig.10 Interfacial Physical Conditions

Fig.10 illustrates the interfacial physical conditions between two materials, material *1* and material *2*. Material *1* has a modulus of $E_1$ and a Poisson ratio of $\nu_1$; material *2* has a modulus of $E_2$ and a Poisson ratio of $\nu_2$. The displacement field in material *1* is defined by $\{u^{I}(x,y),\ v^{I}(x,y)\}$ and the displacement field in material *2* is defined by $\{u^{II}(x,y),\ v^{II}(x,y)\}$. $u$ denotes displacement in the $x$-direction and $v$ denotes displacement in the $y$-direction. Physical reality at the interface includes:

a. continuity of displacement at the interface,
(Refer to Fig.10. $\{u^{I}(x,y),\ v^{I}(x,y)\} = \{u^{II}(x,y),\ v^{II}(x,y)\}$ along the interface.)
b. discontinuity of normal strains($\varepsilon_n$), shear strains($\gamma_{nt}$) and tangential stress ($\sigma_t$) at the interface, and
c. equilibrium conditions, i.e. continuity of normal stress and shear stress ($\sigma_n^{I} = \sigma_n^{II}$ , $\tau_{nt}^{I} = \tau_{nt}^{II}$ ) at the interface.

Where $\sigma$ denotes normal stress, $\tau$ denotes shear stress, $\varepsilon$ denotes normal strain, $\gamma$ denotes shear strain and subscripts $n$ and $t$ denote normal direction and tangential direction at the interface of two materials, respectively.

A heterogeneous element, in contrast to conventional elements, can contain one or more kinds of materials with different moduli and other mechanical properties. Matching element boundaries to fiber-matrix interfaces is unnecessary. More importantly, heterogeneous element formulations more realistically reflect interfacial physics.

In this project, we developed two heterogeneous element approaches. One is a displacement based element formulation; the other a mixed-form element formulation. For the former, displacement continuity along the interface is guaranteed. Stress equilibrium along the interface is satisfied in a weak form. Discontinuity of normal strains($\varepsilon_n$), shear strains($\gamma_{nt}$) and tangential stress ($\sigma_t$) at the interface can also be modeled. For the latter, all three conditions, continuity of displacement at the interface, discontinuity of normal strains, shear strains and tangential stress at the interface and equilibrium conditions, are strictly satisfied.

Numerical results show the heterogeneous element approach as much more accurate than the conventional iso-parametric and conventional mixed element approaches. It also avoids difficulties inherent to mesh-generation.

## 3.2 Displacement Based Heterogeneous Element

### 3.2.1 Shape Functions

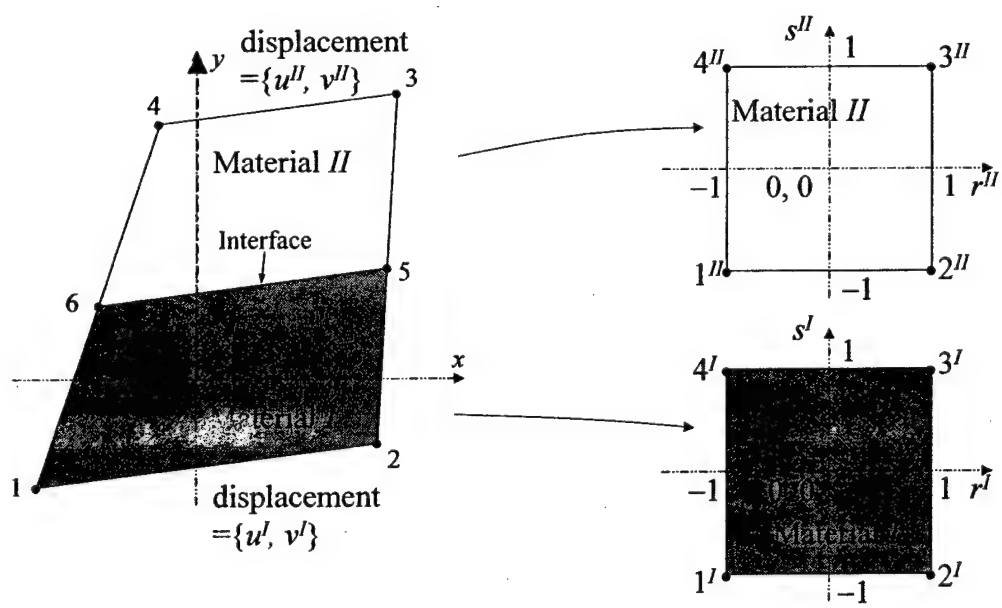


11-a 6-node heterogeneous element 11-b Natural Coordinates

Fig.11 6-Node Standard Heterogeneous Element and Their Natural Coordinate System Mapping

Fig.11 shows a standard 6-node heterogeneous element, referred to as "D6" in this report. The element contains two material parts, materials *I* and *II*. The interface is represented by a straight line intersecting two opposite element sides and creating the two side nodes. Each material part is treated as a sub-element that is mapped to a 2 by 2 square in a natural coordinate system, the *r-s* system. Shape functions are denoted as $H_i^K$, where $i$ = 1, 2, ..., 6, representing element nodal numbers and $K = I, II$, representing the material index. The shape functions are:

| material *I* | material *II* |
|---|---|
| $H_1^I = \frac{1}{4}(1-r)(1-s)$ | $H_6^{II} = \frac{1}{4}(1-r)(1-s)$ |
| $H_2^I = \frac{1}{4}(1+r)(1-s)$ | $H_5^{II} = \frac{1}{4}(1+r)(1-s)$ |
| $H_5^I = \frac{1}{4}(1+r)(1+s)$ | $H_3^{II} = \frac{1}{4}(1+r)(1+s)$ |
| $H_6^I = \frac{1}{4}(1-r)(1+s)$ | $H_4^{II} = \frac{1}{4}(1-r)(1+s)$ |

(3)

The element coordinates are interpolated as:

| material *I* | material *II* |
|---|---|
| $x = \sum_{i=1,2,5,6} H_i^I x_i$ | $x = \sum_{i=6,5,3,4} H_i^{II} x_i$ |
| $y = \sum_{i=1,2,5,6} H_i^I y_i$ | $y = \sum_{i=6,5,3,4} H_i^{II} y_i$ |

(4)

3.2.2 Displacement Functions

<u>Degrees of Freedom</u>

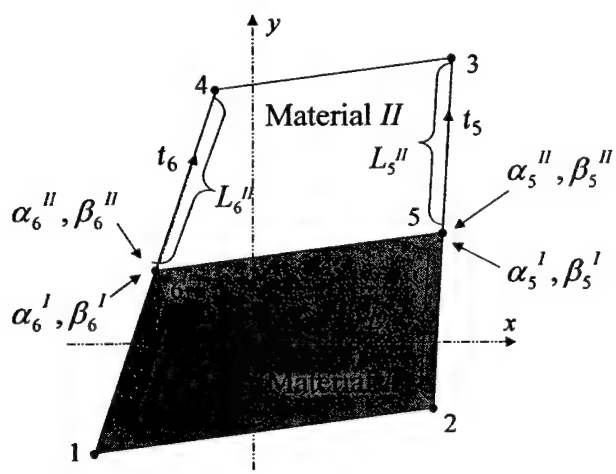


Fig.12 Additional Degrees of Freedom

If iso-parametric displacement functions are applied to each sub-element shown in Fig.11, the stress equilibrium conditions between the two materials cannot be satisfied. In order to address stress equilibrium conditions, two additional degrees of freedom are introduced to the sub-element node at the interface, $\alpha_i^K$ and $\beta_i^K$ ($i = 5, 6$ and $K = I, II$), where $K$ is the material index and $i$ is the nodal number. $\alpha_i^K$ and $\beta_i^K$ are defined as derivatives of displacements $u$ and $v$ along the tangential direction of the element's left and right side boundaries at the interfacial node, i.e. $\alpha_i^K = \left(\frac{\partial u^K}{\partial t_i}\right)_i$ and $\beta_i^K = \left(\frac{\partial v^K}{\partial t_i}\right)_i$. $t_i$ directions are shown in Fig.12. Since coordinate mapping is linear and $r$ is constant along the element's left and right sides, $\alpha_i^K$ and $\beta_i^K$ can be expressed in terms of natural coordinates, such as:

$$\begin{aligned} \alpha_i^K &= \left(\frac{\partial u^K}{\partial t}\right)_i = \frac{2}{L_i^K}\left(\frac{\partial u^K}{\partial s}\right)_i \\ \beta_i^K &= \left(\frac{\partial v^K}{\partial t}\right)_i = \frac{2}{L_i^K}\left(\frac{\partial v^K}{\partial s}\right)_i \end{aligned} \tag{5}$$

where $L_i^K$ is the side length of the element shown in Fig.12.

Displacement Functions

The element displacements in material $I$ and material $II$ are interpolated as:

$$\begin{aligned} &\text{Material } I && \text{Material } II \\ u^I &= \sum_{i=1,2,5,6} N_i^I u_i + \sum_{i=5,6} M_i^I \alpha_i^I && u^{II} = \sum_{i=6,5,3,4} N_i^{II} u_i + \sum_{i=6,5} M_i^{II} \alpha_i^{II} \\ v^I &= \sum_{i=1,2,5,6} N_i^I v_i + \sum_{i=5,6} M_i^I \beta_i^I && v^{II} = \sum_{i=6,5,3,4} N_i^{II} v_i + \sum_{i=6,5} M_i^{II} \beta_i^{II} \end{aligned} \tag{6}$$

where $N_i^I$, $M_i^I$, $N_i^{II}$, $M_i^{II}$ are displacement interpolation functions of material $I$ and material $II$. They can be expressed as:

$$\begin{aligned} &\text{Material } I && \text{Material } II \\ N_1^I &= \tfrac{1}{8}(1-r)(1-s)^2 && N_6^{II} = \tfrac{1}{8}(1-r)(3+s)(1-s) \\ N_2^I &= \tfrac{1}{8}(1+r)(1-s)^2 && N_5^{II} = \tfrac{1}{8}(1+r)(3+s)(1-s) \\ N_5^I &= \tfrac{1}{8}(1+r)(3-s)(1+s) && N_3^{II} = \tfrac{1}{8}(1+r)(1+s)^2 \\ N_6^I &= \tfrac{1}{8}(1-r)(3-s)(1+s) && N_4^{II} = \tfrac{1}{8}(1-r)(1+s)^2 \\ M_5^I &= -\frac{L_5^I}{8}(1+r)(1-s^2) && M_6^{II} = \frac{L_6^{II}}{8}(1-r)(1-s^2) \\ M_6^I &= -\frac{L_6^I}{8}(1-r)(1-s^2) && M_5^{II} = \frac{L_5^{II}}{8}(1+r)(1-s^2) \end{aligned} \tag{7}$$

It can be proved that the above displacement functions satisfy the unit properties, i.e.,

1. At any node $j$, $j = 1,2,\ldots,6$,

$$N_i^K = 0 \quad if \quad i \neq j \quad \text{and} \quad N_i^K = 1 \quad if \quad i = j$$
$$M_i^K = 0 \tag{8-a}$$

2. At interfacial nodes 5 and 6,

$$\frac{\partial M_i^I}{\partial t_j} = 0 \quad if \quad i \neq j \quad \text{and} \quad \frac{\partial M_i^I}{\partial t_j} = 1 \quad if \quad i = j$$
$$\frac{\partial N_i^I}{\partial t_j} = 0 \tag{8-b}$$

In addition, the continuity of displacement at the interface is automatically satisfied. It is not difficult to prove $\{u^I(x,y), v^I(x,y)\} = \{u^{II}(x,y), v^{II}(x,y)\}$ along the interface.

Stress and Strain

The strains in each material can be derived by differentiating displacements $u$ and $v$ with respect to coordinates $x$ and $y$ as:

$$\varepsilon^I = \begin{Bmatrix} \varepsilon_x \\ \varepsilon_y \\ \gamma_{xy} \end{Bmatrix}^I = \begin{Bmatrix} \dfrac{\partial u}{\partial x} \\ \dfrac{\partial v}{\partial y} \\ \dfrac{\partial u}{\partial y} + \dfrac{\partial v}{\partial x} \end{Bmatrix}^I = \begin{bmatrix} \underset{3\times 12}{\mathbf{B}_U^I} & \underset{3\times 2}{\mathbf{B}_{\Lambda 5}^I} & \underset{3\times 2}{\mathbf{B}_{\Lambda 6}^I} \end{bmatrix} \begin{Bmatrix} \mathbf{U} \\ \mathbf{\Lambda}_5^I \\ \mathbf{\Lambda}_6^I \end{Bmatrix} \tag{9-a}$$

$$\varepsilon^{II} = \begin{Bmatrix} \varepsilon_x \\ \varepsilon_y \\ \gamma_{xy} \end{Bmatrix}^{II} = \begin{Bmatrix} \dfrac{\partial u}{\partial x} \\ \dfrac{\partial v}{\partial y} \\ \dfrac{\partial u}{\partial y} + \dfrac{\partial v}{\partial x} \end{Bmatrix}^{II} = \begin{bmatrix} \underset{3\times 12}{\mathbf{B}_U^{II}} & \underset{3\times 2}{\mathbf{B}_{\Lambda 5}^{II}} & \underset{3\times 2}{\mathbf{B}_{\Lambda 6}^{II}} \end{bmatrix} \begin{Bmatrix} \mathbf{U} \\ \mathbf{\Lambda}_5^{II} \\ \mathbf{\Lambda}_6^{II} \end{Bmatrix} \tag{9-b}$$

where $\mathbf{U}$ denotes $\{u_1\ v_1\ u_2\ v_2\ u_3\ v_3\ u_4\ v_4\ u_5\ v_5\ u_6\ v_6\}^T$, a vector listing of nodal displacement variables, $\mathbf{\Lambda}_i^K$ denotes vector $\{\alpha_i^K\ \beta_i^K\}^T$ for ($i$ = 5, 6 and $K = I, II$), and $\lfloor \mathbf{B}_U^K \rfloor$ and $\lfloor \mathbf{B}_{\Lambda i}^K \rfloor$ are partial strain-displacement transformation matrices of material $K$ related to variables in $\mathbf{U}$ and in $\mathbf{\Lambda}_i^K$ respectively. Stresses can then be derived by Hooke's Law.

The stresses derived from displacement interpolations are distributed linearly along the interface, and the strain in the $t_i$ direction is linear along the element's left and right sides, as displayed in Fig.13. In order to maintain stress equilibrium at any point on the interface, it is necessary and sufficient to maintain the equilibrium of stresses at both interfacial nodes.

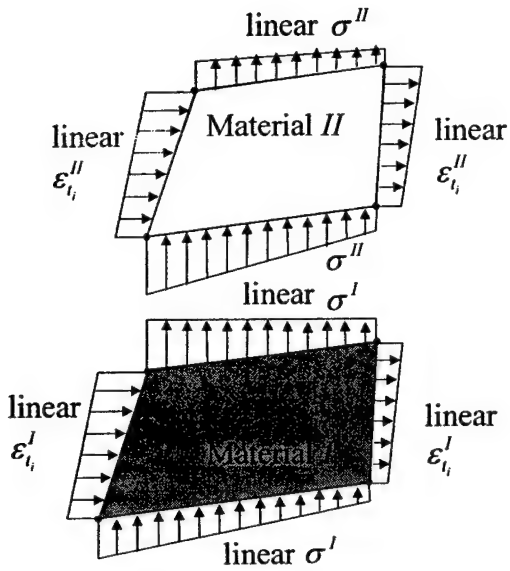


Fig.13 Stress and strain distribution along interface and element boundaries

**Stress along the Interface**

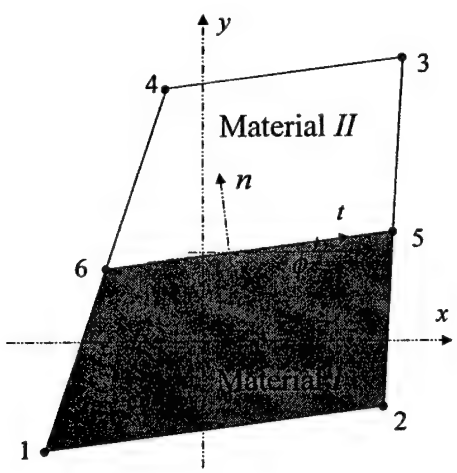


Fig.14 Interfacial co-ordinate system

The interfacial ($t$-$n$) coordinate system is shown in Fig. 14, where $t$ is pointing in the tangential direction of the interface, and $n$ is pointing in the normal interfacial direction. Stresses in the $t$-$n$ coordinate system in each material $K$ ($K = I, II$) can be evaluated by using strain-displacement relations, Hooke's Law, and stress coordinate transformation as follows:

$$\begin{Bmatrix}\sigma_t\\ \sigma_n\\ \tau_{tn}\end{Bmatrix}^K = [\mathbf{T}_\sigma]\begin{Bmatrix}\sigma_x\\ \sigma_y\\ \sigma_{xy}\end{Bmatrix}^K = [\mathbf{T}_\sigma][\mathbf{D}^K]\begin{Bmatrix}\varepsilon_x\\ \varepsilon_y\\ \gamma_{xy}\end{Bmatrix}^K \tag{10}$$

where $[\mathbf{T}_\sigma]$ is the stress transformation matrix, **[D]** is the elastic matrix and K is the material index ($K=I,II$).

<u>Displacement Compatibility between Heterogeneous Elements; Stress Equilibrium along Dissimilar Material Interfaces; Element Stiffness Matrix</u>

There are two stress equilibrium conditions along the interface:

$$\sigma_n^{\ I} = \sigma_n^{\ II} \quad \text{and} \quad \tau_{tn}^{\ I} = \tau_{tn}^{\ II} \tag{11}$$

Since stresses are linear along the interface, satisfaction of stress equilibrium conditions at two interfacial nodes guarantees satisfaction at any point on the interface. The implementation of the two conditions described in eqs. 11 at two interfacial nodes, means the following four stress equations must be satisfied:

Node 5:

$$\underset{2\times3}{[(\mathbf{T}_\sigma)_{2-3}]}\underset{3\times3}{[\mathbf{D}^I]}\Big[\underset{3\times12}{[\mathbf{B}_U^I]_5}\mathbf{U}+\underset{3\times2}{[\mathbf{B}_{\Lambda5}^I]_5}\Lambda_5^I\Big]=\underset{2\times3}{[(\mathbf{T}_\sigma)_{2-3}]}\underset{3\times3}{[\mathbf{D}^{II}]}\Big[\underset{3\times12}{[\mathbf{B}_U^{II}]_5}\mathbf{U}+\underset{3\times2}{[\mathbf{B}_{\Lambda5}^{II}]_5}\Lambda_5^{II}\Big] \tag{12-a}$$

Node 6:

$$\underset{2\times3}{[(\mathbf{T}_\sigma)_{2-3}]}\underset{3\times3}{[\mathbf{D}^I]}\Big[\underset{3\times12}{[\mathbf{B}_U^I]_6}\mathbf{U}+\underset{3\times2}{[\mathbf{B}_{\Lambda6}^I]_6}\Lambda_6^I\Big]=\underset{2\times3}{[(\mathbf{T}_\sigma)_{2-3}]}\underset{3\times3}{[\mathbf{D}^{II}]}\Big[\underset{3\times12}{[\mathbf{B}_U^{II}]_6}\mathbf{U}+\underset{3\times2}{[\mathbf{B}_{\Lambda6}^{II}]_6}\Lambda_6^{II}\Big] \tag{12-b}$$

in which $[(\mathbf{T}_\sigma)_{2-3}]$ denotes the matrix that contains the 2nd and 3rd rows of matrix $[\mathbf{T}_\sigma]$. $\mathbf{\Lambda}_5^K$ ($K=I, II$) does not affect stresses at node 6 and vice versa.

The above four equations restrict the four degrees of freedom; thus, $\mathbf{\Lambda}_i^I$ and $\mathbf{\Lambda}_i^{II}$ are not independent degrees of freedom given the interfacial stress equilibrium equations (12-a) and (12-b) are considered. Once $\mathbf{\Lambda}_i^I$ is determined, $\mathbf{\Lambda}_i^{II}$ can be derived using Eqs.(12).

Refer to Fig. 15. In order to maintain displacement compatibility between two adjacent heterogeneous elements, e.g., element A and element B, the following relationship must be satisfied:

$$\begin{aligned}(\mathbf{\Lambda}_5^I)^A &= (\mathbf{\Lambda}_6^I)^B\\ (\mathbf{\Lambda}_5^{II})^A &= (\mathbf{\Lambda}_6^{II})^B\end{aligned} \tag{13}$$

However, if $(\mathbf{\Lambda}_5^I)^A = (\mathbf{\Lambda}_6^I)^B$, $(\mathbf{\Lambda}_5^{II})^A$ and $(\mathbf{\Lambda}_6^{II})^B$ can be derived from stress equilibrium conditions, that are Eqs.(12) for element A and B, respectively. The derived $(\mathbf{\Lambda}_5^{II})^A$ and $(\mathbf{\Lambda}_6^{II})^B$ can not equal each other. This means the interfacial stress equilibrium and the compatibility between two adjacent heterogeneous elements can not be satisfied simultaneously.

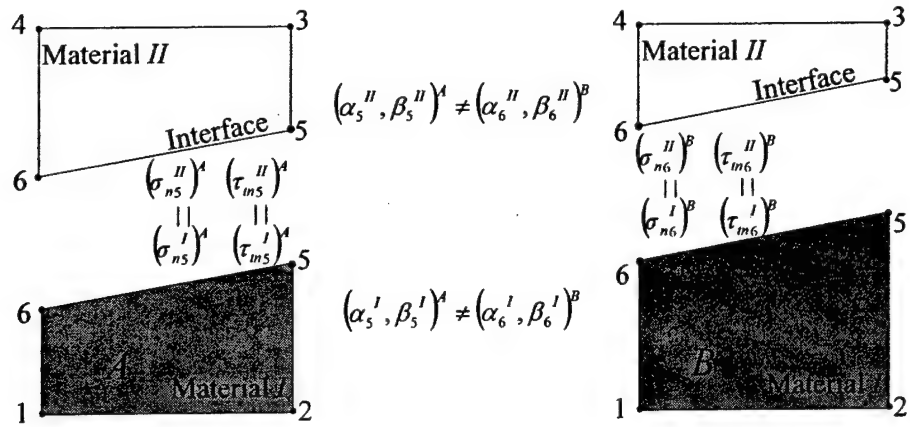


15-a Maintain Interfacial Equilibrium and Compromise Displacement Compatibility

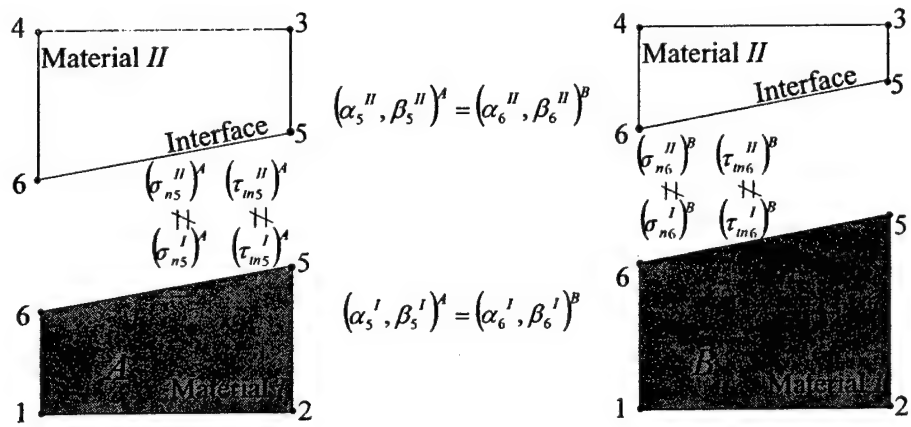


15-b Maintain Displacement Compatibility and Compromise Interfacial Equilibrium

Fig.15 Displacement compatibility and interfacial equilibrium conditions

A weak form of interfacial equilibrium conditions is developed in order to maintain displacement continuity between adjacent heterogeneous elements. Refer to Fig.16. For each element, instead of using the continuity of normal and shear stresses at nodes 5 and 6, an average of the equilibrium conditions at an interfacial node for the adjacent elements is used. For example, on the interfacial node between $A$ and $B$, a weak form of the equilibrium conditions can be expressed as:

$$\begin{aligned}(\sigma_{n5}^{I})^A + (\sigma_{n6}^{I})^B &= (\sigma_{n5}^{II})^A + (\sigma_{n6}^{II})^B \\ (\tau_{tn5}^{I})^A + (\tau_{tn6}^{I})^B &= (\tau_{tn5}^{II})^A + (\tau_{tn6}^{II})^B\end{aligned} \tag{14}$$

Through mathematical manipulation, a weak form of the equilibrium conditions becomes:

$$[\mathbf{S}_U]_5^A \mathbf{U}^A + [\mathbf{S}_U]_6^B \mathbf{U}^B + [\mathbf{S}_\Lambda^I]_5^A (\mathbf{\Lambda}_5^I)^A + [\mathbf{S}_\Lambda^I]_6^B (\mathbf{\Lambda}_6^I)^B - [\mathbf{S}_\Lambda^{II}]_5^A (\mathbf{\Lambda}_5^{II})^A - [\mathbf{S}_\Lambda^{II}]_6^B (\mathbf{\Lambda}_6^{II})^B = 0 \tag{15}$$

where $[\mathbf{S}_U]_5^A, [\mathbf{S}_U]_6^B, [\mathbf{S}_\Lambda^I]_5^A, [\mathbf{S}_\Lambda^I]_6^B, [\mathbf{S}_\Lambda^{II}]_5^A$ and $[\mathbf{S}_\Lambda^{II}]_6^B$ are derived from

$$
\begin{aligned}
[\mathbf{S}_U]_i^e &= [(\mathbf{T}_\sigma)_{2-3}]^e \left([\mathbf{D}^I][\mathbf{B}_U^I] - [\mathbf{D}^{II}][\mathbf{B}_U^{II}]\right)_i^e \\
[\mathbf{S}_\Lambda^K]_i^e &= [(\mathbf{T}_\sigma)_{2-3}]^e [\mathbf{D}^K][\mathbf{B}_{\Lambda i}^K]_i^e
\end{aligned}
\tag{16}
$$

where $K = I, II$, $e = A, B$ and $i = 5, 6$. Assuming $(\mathbf{\Lambda}_6^I)^B = (\mathbf{\Lambda}_5^I)^A$ and $(\mathbf{\Lambda}_6^{II})^B = (\mathbf{\Lambda}_5^{II})^A$, one derives:

$$
[\mathbf{S}_U]_5^A \mathbf{U}^A + [\mathbf{S}_U]_6^B \mathbf{U}^B + \left([\mathbf{S}_\Lambda^I]_5^A + [\mathbf{S}_\Lambda^I]_6^B\right)(\mathbf{\Lambda}_5^I)^A - \left([\mathbf{S}_\Lambda^{II}]_5^A + [\mathbf{S}_\Lambda^{II}]_6^B\right)(\mathbf{\Lambda}_5^{II})^A = 0 \tag{17}
$$

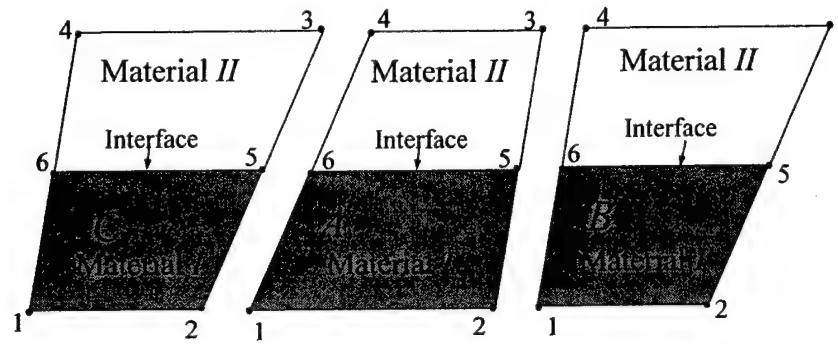


Fig.16 Element A is adjacent to elements *B* and C

Therefore, $(\mathbf{\Lambda}_5^I)^A$ and $(\mathbf{\Lambda}_5^{II})^A$ is dependent on each other. Without loss of generosity, assume $(\mathbf{\Lambda}_5^I)^A$ is an independent variable and $(\mathbf{\Lambda}_5^{II})^A$ is a dependent variable, which can be expressed as:

$$
(\mathbf{\Lambda}_5^{II})^A = \left([\mathbf{S}_\Lambda^{II}]_5^A + [\mathbf{S}_\Lambda^{II}]_6^B\right)^{-1} \left([\mathbf{S}_U]_5^A \mathbf{U}^A + [\mathbf{S}_U]_6^B \mathbf{U}^B + \left([\mathbf{S}_\Lambda^I]_5^A + [\mathbf{S}_\Lambda^I]_6^B\right)(\mathbf{\Lambda}_5^I)^A\right) \tag{18-a}
$$

Following exactly the same procedure, dependent variables $(\mathbf{\Lambda}_6^{II})^A$ is shared by elements *A* and *C*, which can be expressed as:

$$
(\mathbf{\Lambda}_6^{II})^A = \left([\mathbf{S}_\Lambda^{II}]_5^C + [\mathbf{S}_\Lambda^{II}]_6^A\right)^{-1} \left([\mathbf{S}_U]_5^C \mathbf{U}^C + [\mathbf{S}_U]_6^A \mathbf{U}^A + \left([\mathbf{S}_\Lambda^I]_5^C + [\mathbf{S}_\Lambda^I]_6^A\right)(\mathbf{\Lambda}_6^I)^A\right) \tag{18-b}
$$

Dependent variables can be eliminated in strain-displacement relations and element stiffness matrices. Substituting Eqs.(18) into Eqs.(9), the strain-displacement relations are be expressed as

$$\varepsilon^{I} = \begin{bmatrix} \mathbf{B}_U^I & \mathbf{0} & \mathbf{0} & \mathbf{B}_{\Lambda 5}^I & \mathbf{B}_{\Lambda 6}^I \end{bmatrix} \begin{Bmatrix} \mathbf{U}^A \\ \mathbf{U}^B \\ \mathbf{U}^C \\ \mathbf{\Lambda}_5^I \\ \mathbf{\Lambda}_6^I \end{Bmatrix}$$

$$\varepsilon^{II} = \begin{bmatrix} \left(\mathbf{B}_U^{II}\right)^A & \left(\mathbf{B}_U^{II}\right)^B & \left(\mathbf{B}_U^{II}\right)^C & \left(\mathbf{B}_{\Lambda 5}^{II}\right)^{A-B} & \left(\mathbf{B}_{\Lambda 6}^{II}\right)^{C-A} \end{bmatrix} \begin{Bmatrix} \mathbf{U}^A \\ \mathbf{U}^B \\ \mathbf{U}^C \\ \mathbf{\Lambda}_5^I \\ \mathbf{\Lambda}_6^I \end{Bmatrix} \tag{19}$$

where

$$\begin{aligned}
\left[\mathbf{B}_U^{II}\right]^A &= \left[\mathbf{B}_U^{II}\right] + \left[\mathbf{B}_{\Lambda 5}^{II}\right]\left(\left[\mathbf{S}_\Lambda^{II}\right]_5^A + \left[\mathbf{S}_\Lambda^{II}\right]_6^B\right)^{-1}\left[\mathbf{S}_U\right]_5^A + \left[\mathbf{B}_{\Lambda 6}^{II}\right]\left(\left[\mathbf{S}_\Lambda^{II}\right]_5^C + \left[\mathbf{S}_\Lambda^{II}\right]_6^A\right)^{-1}\left[\mathbf{S}_U\right]_6^A \\
\left[\mathbf{B}_U^{II}\right]^B &= \left[\mathbf{B}_{\Lambda 5}^{II}\right]\left(\left[\mathbf{S}_\Lambda^{II}\right]_5^A + \left[\mathbf{S}_\Lambda^{II}\right]_6^B\right)^{-1}\left[\mathbf{S}_U\right]_6^B \\
\left[\mathbf{B}_U^{II}\right]^C &= \left[\mathbf{B}_{\Lambda 6}^{II}\right]\left(\left[\mathbf{S}_\Lambda^{II}\right]_5^C + \left[\mathbf{S}_\Lambda^{II}\right]_6^A\right)^{-1}\left[\mathbf{S}_U\right]_5^C \\
\left[\mathbf{B}_{\Lambda 5}^{II}\right]^{A-B} &= \left[\mathbf{B}_{\Lambda 5}^{II}\right]\left(\left[\mathbf{S}_\Lambda^{II}\right]_5^A + \left[\mathbf{S}_\Lambda^{II}\right]_6^B\right)^{-1}\left(\left[\mathbf{S}_\Lambda^{I}\right]_5^A + \left[\mathbf{S}_\Lambda^{I}\right]_6^B\right) \\
\left[\mathbf{B}_{\Lambda 6}^{II}\right]^{C-A} &= \left[\mathbf{B}_{\Lambda 6}^{II}\right]\left(\left[\mathbf{S}_\Lambda^{II}\right]_5^C + \left[\mathbf{S}_\Lambda^{II}\right]_6^A\right)^{-1}\left(\left[\mathbf{S}_\Lambda^{I}\right]_5^C + \left[\mathbf{S}_\Lambda^{I}\right]_6^A\right)
\end{aligned} \tag{20}$$

The element stiffness matrix $K$ can be derived as:

$$\begin{aligned}
[\mathbf{K}] = &\int_I \left[\mathbf{B}_U^I \;\; \mathbf{0} \;\; \mathbf{0} \;\; \mathbf{B}_{\Lambda 5}^I \; \mathbf{B}_{\Lambda 6}^I\right]^T \left[\mathbf{D}^I\right]\left[\mathbf{B}_U^I \;\; \mathbf{0} \;\; \mathbf{0} \;\; \mathbf{B}_{\Lambda 5}^I \; \mathbf{B}_{\Lambda 6}^I\right] ds \\
&+ \int_{II} \left[\left(\mathbf{B}_U^{II}\right)^A \left(\mathbf{B}_U^{II}\right)^B \left(\mathbf{B}_U^{II}\right)^C \left(\mathbf{B}_{\Lambda 5}^{II}\right)^{A-B} \left(\mathbf{B}_{\Lambda 6}^{II}\right)^{C-A}\right]^T \left[\mathbf{D}^{II}\right]\left[\left(\mathbf{B}_U^{II}\right)^A \left(\mathbf{B}_U^{II}\right)^B \left(\mathbf{B}_U^{II}\right)^C \left(\mathbf{B}_{\Lambda 5}^{II}\right)^{A-B} \left(\mathbf{B}_{\Lambda 6}^{II}\right)^{C-A}\right] ds
\end{aligned} \tag{21}$$

**Stress Boundary Conditions**

The distributed load applied to the boundary is transferred into equivalent nodal forces based upon the Virtual Work Principle. Fig.17 shows an example. The distributed stress in the $x$ direction is applied to each material at element boundary 2-5-3. The virtual work done by the forces on virtual displacement $\delta u$ is:

$$
\begin{aligned}
\delta w^I &= \int_{x_2,y_2}^{x_5,y_5} q^I(r,s)\delta u^I(r,s)dl^I \\
&= \frac{q^I L_5^I}{2}\int_{-1}^{1}\delta u^I(r=1,s)ds \\
&= \frac{q^I L_5^I}{2}\int_{-1}^{1}\left[\tfrac{1}{4}(1-s)^2\delta u_2 + \tfrac{1}{4}(3-s)(1+s)\delta u_5 - \tfrac{1}{2}(1-s^2)/Mc_5{}^I\delta\alpha_5{}^I\right]ds \\
&= \frac{q^I L_5^I}{3}\delta u_2 + \frac{2q^I L_5^I}{3}\delta u_5 - \frac{q^I\left(L_5^I\right)^2}{6}\delta\alpha_5{}^I
\end{aligned}
\tag{22-a}
$$

$$
\begin{aligned}
\delta w^{II} &= \int_{x_5,y_5}^{x_3,y_3} q^{II}(r,s)\delta u^{II}(r,s)dl^{II} \\
&= \frac{q^{II} L_5^{II}}{2}\int_{-1}^{1}\delta u^{II}(r=1,s)ds \\
&= \frac{q^{II} L_5^{II}}{2}\int_{-1}^{1}\left[\tfrac{1}{4}(3+s)(1-s)\delta u_5 + \tfrac{1}{4}(1+s)^2\delta u_3 + \tfrac{1}{2}(1-s^2)\delta\alpha_5{}^{II}/Mc_5{}^{II}\right]ds \\
&= \frac{2q^{II} L_5^{II}}{3}\delta u_5 + \frac{q^{II} L_5^{II}}{3}\delta u_3 + \frac{q^{II}\left(L_5^{II}\right)^2}{6}\delta\alpha_5{}^{II}
\end{aligned}
\tag{22-b}
$$

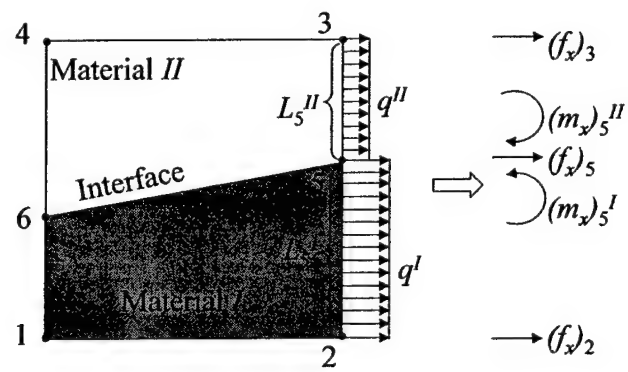


Fig.17 Equivalent nodal forces for the heterogeneous element based on the Principle of Virtual Work

Therefore, according to the Principle of Virtual Work, the equivalent nodal forces are:

$$
\begin{aligned}
&(f_x)_2 = \frac{q^I L_5^I}{3}; \qquad (f_x)_5 = \frac{2q^I L_5^I}{3} + \frac{2q^{II} L_5^{II}}{3}; \qquad (f_x)_3 = \frac{q^{II} L_5^{II}}{3} \\
&(m_x)_5{}^I = -\frac{q^I\left(L_5^I\right)^2}{6}, \quad (m_x)_5{}^{II} = \frac{q^{II}\left(L_5^{II}\right)^2}{6}
\end{aligned}
\tag{23}
$$

where $(f_x)_i$ is the force on displacement $u_i$, and $(m_x)_i^K$ is the generalized force on displacement derivative $\alpha_i^K$.

The equivalent forces on dependent variables $\Lambda_5^{II}$ and $\Lambda_6^{II}$ are transferred onto other

independent variables based on the Principle of Virtual Work. Assume $\mathbf{M}_5^{II}$ is a vector listing of forces on dependent variables $\mathbf{\Lambda}_5^{II}$. Refer to Eq.(18-a). Replacing $\left[\mathbf{S}_\Lambda^{II}\right]_6^B$, $\left[\mathbf{S}_U\right]_6^B$, and $\left[\mathbf{S}_\Lambda^{I}\right]_6^B$ with zero and replacing $\left[\mathbf{S}_\Lambda^{II}\right]_5^A$, $\left[\mathbf{S}_U\right]_5^A$, and $\left[\mathbf{S}_\Lambda^{I}\right]_5^A$ with $\left[\mathbf{S}_\Lambda^{II}\right]_5$, $\left[\mathbf{S}_U\right]_5$, and $\left[\mathbf{S}_\Lambda^{I}\right]_5$ , Eq.(18-a) becomes:

$$\left(\mathbf{\Lambda}_5^{II}\right) = \left(\left[\mathbf{S}_\Lambda^{II}\right]_5\right)^{-1}\left(\left[\mathbf{S}_U\right]_5\mathbf{U} + \left[\mathbf{S}_\Lambda^{I}\right]_5\left(\mathbf{\Lambda}_5^{I}\right)\right) \tag{24}$$

The virtual work by $\mathbf{M}_5^{II}$ on virtual displacement $\delta\mathbf{\Lambda}_5^{II}$ is:

$$\left[\mathbf{M}_5{}^{II}\right]^T\delta\mathbf{\Lambda}_5^{II} = \left[\mathbf{M}_5{}^{II}\right]^T\left(\left[\mathbf{S}_\Lambda^{II}\right]_5\right)^{-1}\left(\left[\mathbf{S}_U\right]_5\delta\mathbf{U} + \left[\mathbf{S}_\Lambda^{I}\right]_5\left(\delta\mathbf{\Lambda}_5^{I}\right)\right) \tag{25}$$

Then, $\left[\mathbf{M}_5^{II}\right]^T\left(\left[\mathbf{S}_\Lambda^{II}\right]_5\right)^{-1}\left[\mathbf{S}_U\right]_5$ and $\left[\mathbf{M}_5^{II}\right]^T\left(\left[\mathbf{S}_\Lambda^{II}\right]_5\right)^{-1}\left[\mathbf{S}_\Lambda^{I}\right]_5$ are added onto nodal forces corresponding to variables $\mathbf{U}$ and $\Lambda_5^I$ respectively.

Displacement Based Heterogeneous Element with Different Interface Locations

The interface can be located in many places in a displacement based heterogeneous element. For the convenience of mesh generation , six elements with different interface locations are derived, as shown in Fig.18. They are formulated using exactly the same process as the 6-node standard element; only the node mapping sequence from the element coordinate system to its natural coordinate system is different. Details can be found in reference [2].

Convergence Properties

Displacement functions of displacement based heterogeneous elements can represent all rigid body displacement modes and represent constant stress and strain states. They are complete. Further, displacement compatibility is guaranteed along the interface between adjacent heterogeneous elements. In addition, they are compatible with the neighboring iso-parametrical elements. Heterogeneous element formulation, therefore, satisfies the condition for monotonic convergence. Numerical results show that it converges at a much faster rate than conventional iso-parametric elements.

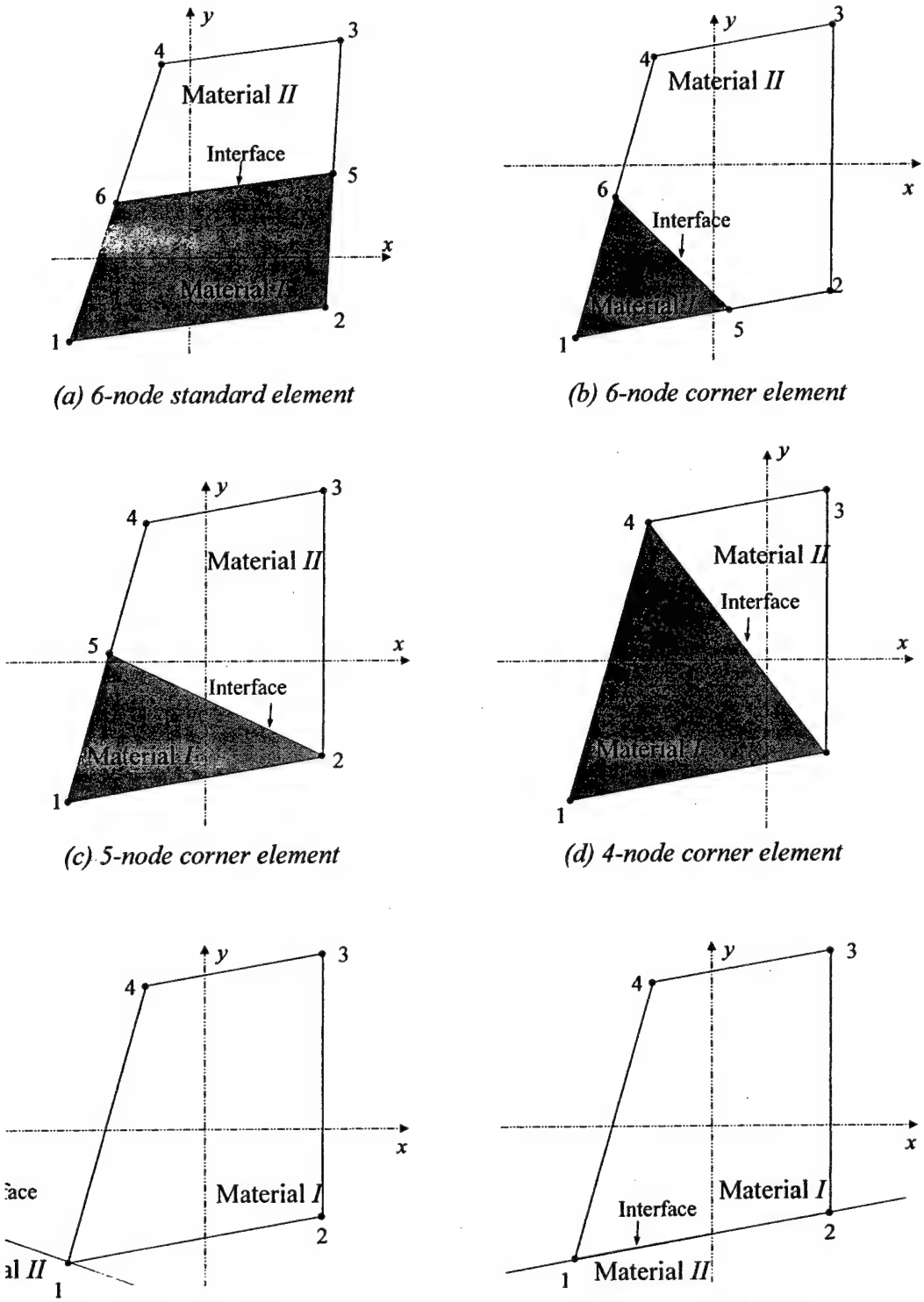


Fig.18 2-D displacement-based heterogeneous elements

## 3.3 Mixed Heterogeneous Elements

As has been explained, a displacement based heterogeneous element formulation can only satisfy a weak form of interfacial equilibrium conditions. For this reason, a second mixed form of heterogeneous element is developed. This formulation enables enforcement of interfacial equilibrium conditions and compatibility conditions.

There are two kinds of stress interpolation functions used in mixed elements:

1. The $u/\sigma$-$c$ formulation ($c$ stands for continuity of stresses between elements), in which element stresses are defined by nodal stress variables, and iso-parametric interpolation functions;
2. The $u/\sigma$ formulation, in which stress variables are local. Continuity of stress is not enforced between elements but results from the solution of the finite element if the mesh is fine enough.

The first stress formulation can represent the continuity of normal stress (traction force) and shear stress along the dissimilar material interface, but cannot reflect the tangential stress jump along the interface. The second approach allows for the tangential stress jump, but cannot satisfy the continuity of normal stress and shear stress along the interface.

The heterogeneous element formulation developed in this project modifies the second approach. It guarantees the continuity of normal and shear stress along the interface, yet it also allows for the tangential stress jump between two materials. In addition, the displacement function guarantees compatibility along the interface and between elements. Using this mixed element approach, the material's constitutive relations, i.e., Hooke's Law, is realized through Reissner's Variational Principle.

### 3.3.1 Mixed Heterogeneous Element Formulations

For the mixed heterogeneous formulation, the key issue is how to construct the displacement and stress interpolation functions. The stress interpolation should not be of too high an order compared to the displacement interpolation, for the element could again behave like a displacement-based element, so be ineffective. On the other hand, the stress interpolation should not be too low an order compared to the displacement interpolation, for the stress prediction could be too inaccurate. Generally, stress interpolation functions are of a lower order than displacement interpolation functions because actual stresses are found through strains as derivatives of displacements.

**<u>Shape Functions, Displacement Functions and Strain-displacement relations</u>**

Refer to Fig. 19. A standard mixed heterogeneous element contains two sub-elements, each being composed from a material, material $I$ and material $II$, respectively. Shape functions and displacement functions of mixed heterogeneous elements are the same as displacement based heterogeneous elements, which are expressed by Eqs.(9) and can be written as:

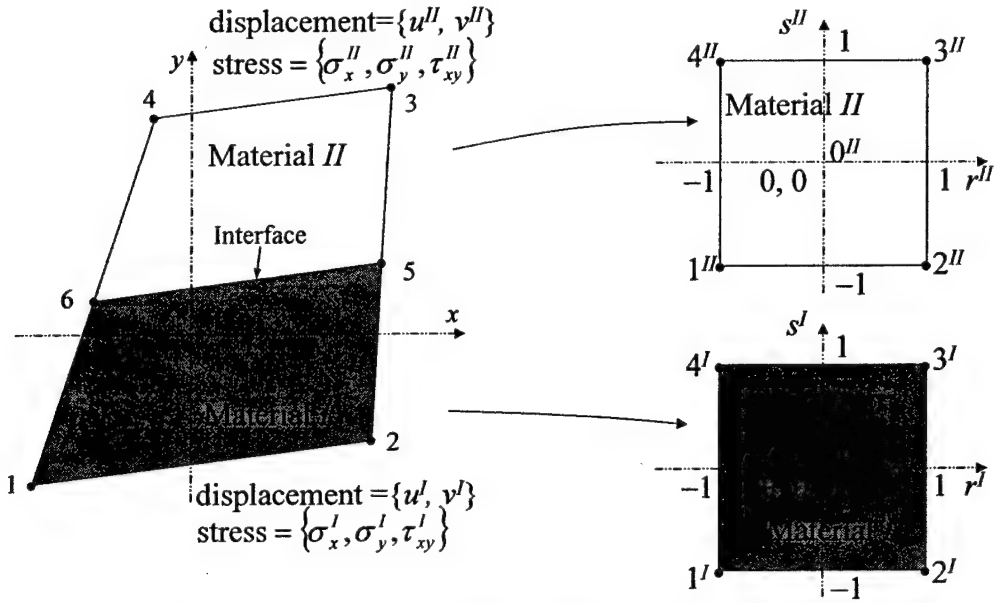


Fig.19 6-node Standard Mixed Heterogeneous Element
with Natural Coordinate System Mapping

$$\varepsilon^I = \begin{Bmatrix} \varepsilon_x \\ \varepsilon_y \\ \gamma_{xy} \end{Bmatrix}^I = \begin{Bmatrix} \dfrac{\partial u}{\partial x} \\ \dfrac{\partial v}{\partial y} \\ \dfrac{\partial u}{\partial y} + \dfrac{\partial v}{\partial x} \end{Bmatrix}^I = \underset{3\times12}{\left[\mathbf{B}_U^I\right.} \underset{3\times2}{\mathbf{B}_{\Lambda 5}^I} \underset{3\times2}{\left.\mathbf{B}_{\Lambda 6}^I\right]} \begin{Bmatrix} \mathbf{U} \\ \mathbf{\Lambda}_5^I \\ \mathbf{\Lambda}_6^I \end{Bmatrix} = [\mathbf{B}^I]\mathbf{V} \tag{26-a}$$

$$\varepsilon^{II} = \begin{Bmatrix} \varepsilon_x \\ \varepsilon_y \\ \gamma_{xy} \end{Bmatrix}^{II} = \begin{Bmatrix} \dfrac{\partial u}{\partial x} \\ \dfrac{\partial v}{\partial y} \\ \dfrac{\partial u}{\partial y} + \dfrac{\partial v}{\partial x} \end{Bmatrix}^{II} = \underset{3\times12}{\left[\mathbf{B}_U^{II}\right.} \underset{3\times2}{\mathbf{B}_{\Lambda 5}^{II}} \underset{3\times2}{\left.\mathbf{B}_{\Lambda 6}^{II}\right]} \begin{Bmatrix} \mathbf{U} \\ \mathbf{\Lambda}_5^{II} \\ \mathbf{\Lambda}_6^{II} \end{Bmatrix} = [\mathbf{B}^{II}]\mathbf{V} \tag{26-b}$$

where $\mathbf{V}$ is $\{u_1\ v_1\ u_2\ v_2\ u_3\ v_3\ u_4\ v_4\ u_5\ v_5\ u_6\ v_6\ \alpha_5^I\ \beta_5^I\ \alpha_6^I\ \beta_6^I\ \alpha_5^{II}\ \beta_5^{II}\ \alpha_6^{II}\ \beta_6^{II}\}^T$, a vector listing of all displacement variables, and where $[\mathbf{B}^I]$ and $[\mathbf{B}^I]$ are the strain-displacement transformation matrices for material *I* and *II*, respectively.

## Stress Functions

Stress interpolation functions are one degree lower than displacement functions. They are defined as:

| Material $I$ | Material $II$ |
|---|---|
| $\sigma_x{}^I = \sum_{i=0,5,6} M_i^I (\sigma_x)_i^I$ | $\sigma_x{}^{II} = \sum_{i=0,5,6} M_i^{II} (\sigma_x)_i^{II}$ |
| $\sigma_y{}^I = \sum_{i=0,5,6} M_i^I (\sigma_y)_i^I$ | $\sigma_y{}^{II} = \sum_{i=0,5,6} M_i^{II} (\sigma_y)_i^{II}$ |
| $\tau_{xy}{}^I = \sum_{i=0,5,6} M_i^I (\tau_{xy})_i^I$ | $\tau_{xy}{}^{II} = \sum_{i=0,5,6} M_i^{II} (\tau_{xy})_i^{II}$ |

(27)

where $(\sigma_x)_0{}^I$, $(\sigma_x)_5{}^I$, and $(\sigma_x)_6{}^I$ denote stresses at the sub-element center ($r=0$, $s=0$), node 5 and node 6 for material $I$, respectively. Similarly, $(\sigma_x)_0{}^{II}$, $(\sigma_x)_5{}^{II}$, and $(\sigma_x)_6{}^{II}$ denote stresses at the sub-element center ($r=0$, $s=0$), node 5 and node 6 for material $II$, respectively. They can be written as:

$$
\begin{aligned}
(\sigma_x)_0{}^I &= (\sigma_x)^I\Big|_{r=0,s=0} & (\sigma_x)_0{}^{II} &= (\sigma_x)^{II}\Big|_{r=0,s=0} \\
(\sigma_x)_5{}^I &= (\sigma_x)^I\Big|_{r=1,s=1} & (\sigma_x)_5{}^{II} &= (\sigma_x)^{II}\Big|_{r=1,s=1} \\
(\sigma_x)_6{}^I &= (\sigma_x)^I\Big|_{r=-1,s=1} & (\sigma_x)_6{}^{II} &= (\sigma_x)^{II}\Big|_{r=-1,s=1}
\end{aligned}
\tag{28}
$$

$M_i^I$ and $M_i^{II}$ are the interpolation functions. They can be expressed as

| Material $I$ | Material $II$ |
|---|---|
| $M_0^I = 1 - s$ | $M_0^{II} = 1 + s$ |
| $M_5^I = \frac{1}{2}(r + s)$ | $M_5^{II} = -\frac{1}{2}(-r + s)$ |
| $M_6^I = \frac{1}{2}(-r + s)$ | $M_6^{II} = -\frac{1}{2}(r + s)$ |

(29)

It can be proved that the above stress interpolation functions satisfy the unity property similar to Eqs.(8-a).

Eqs.(27) can be expressed in matrix form as:

$$
\sigma^I = \begin{Bmatrix} \sigma_x \\ \sigma_y \\ \tau_{xy} \end{Bmatrix}^I = \begin{bmatrix} \mathbf{M}_0^I & \mathbf{M}_5^I & \mathbf{M}_6^I \end{bmatrix} \begin{Bmatrix} \boldsymbol{\sigma}_0^I \\ \boldsymbol{\sigma}_5^I \\ \boldsymbol{\sigma}_6^I \end{Bmatrix} \tag{30-a}
$$

$$
\sigma^{II} = \begin{Bmatrix} \sigma_x \\ \sigma_y \\ \tau_{xy} \end{Bmatrix}^{II} = \begin{bmatrix} \mathbf{M}_0^{II} & \mathbf{M}_5^{II} & \mathbf{M}_6^{II} \end{bmatrix} \begin{Bmatrix} \boldsymbol{\sigma}_0^{II} \\ \boldsymbol{\sigma}_5^{II} \\ \boldsymbol{\sigma}_6^{II} \end{Bmatrix} \tag{30-b}
$$

Refer to Fig.20. Stress functions expressed in eqs. (30) are linear functions along the interface and the boundary of the element. Based upon the strain functions expressed in eqs. (26), both

normal and tangential strains are linearly distributed along the interface. In addition, tangential strain distributes linearly along the left and right boundaries of the element.

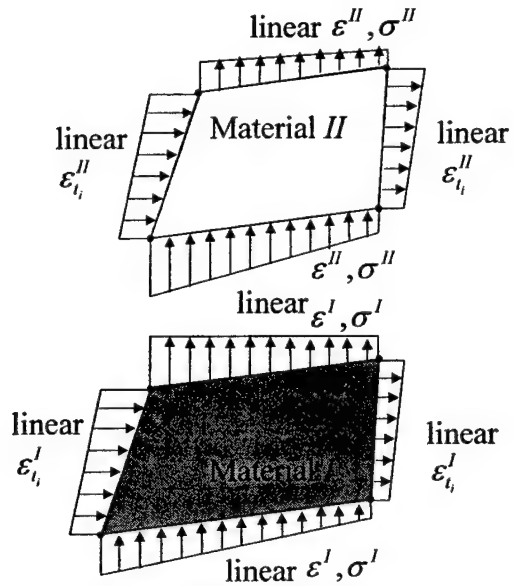


Fig.20 Stress and Strain Distribution along the Element Boundary and Interface

Interfacial Stress Equilibrium Conditions

Stress along interface coordinates can be derived similarly. Refer to Fig.14. Stress along the interface can be written as

$$\begin{Bmatrix} \sigma_t \\ \sigma_n \\ \tau_{tn} \end{Bmatrix}^{I} = [\mathbf{T}_\sigma] \begin{Bmatrix} \sigma_x \\ \sigma_y \\ \sigma_{xy} \end{Bmatrix}^{I} \quad \text{and} \quad \begin{Bmatrix} \sigma_t \\ \sigma_n \\ \tau_{tn} \end{Bmatrix}^{II} = [\mathbf{T}_\sigma] \begin{Bmatrix} \sigma_x \\ \sigma_y \\ \sigma_{xy} \end{Bmatrix}^{II} \tag{31}$$

where $[\mathbf{T}_\sigma]$ is the stress transformation matrix.

There are two equilibrium conditions that need to be maintained at the interface in order to reflect physical conditions there:

1. $\sigma_n^{\ I} = \sigma_n^{\ II}$;
2. $\tau_{tn}^{\ I} = \tau_{tn}^{\ II}$.

Since the stress functions are linear functions along the interface, satisfaction of the two conditions at two interfacial nodes guarantees satisfaction at any point on the interface. Implementation of the two conditions at both interfacial nodes gives rise to four stress equations:

$$\begin{Bmatrix}\sigma_n\\ \tau_{tn}\end{Bmatrix}_5^{I} = \begin{Bmatrix}\sigma_n\\ \tau_{tn}\end{Bmatrix}_5^{II} \quad , \quad and \quad \begin{Bmatrix}\sigma_n\\ \tau_{tn}\end{Bmatrix}_6^{I} = \begin{Bmatrix}\sigma_n\\ \tau_{tn}\end{Bmatrix}_6^{II} \tag{32}$$

Therefore, the four stress variables are dependent variables. They can be eliminated. Combining eqs. (30), (31) and (32), stress within the two materials can be expressed in interfacial coordinates as:

$$\begin{aligned}
\sigma^{I} &= \begin{Bmatrix}\sigma_x\\ \sigma_y\\ \sigma_{xy}\end{Bmatrix}^{I} = \begin{bmatrix}\mathbf{M}_0^{I} & \mathbf{M}_5^{I} & \mathbf{M}_6^{I}\end{bmatrix}\begin{Bmatrix}\boldsymbol{\sigma}_0^{I}\\ \boldsymbol{\sigma}_5^{I}\\ \boldsymbol{\sigma}_6^{I}\end{Bmatrix} = [\mathbf{M}]_{t-n}{}^{I}\{\boldsymbol{\sigma}\}\\
\sigma^{II} &= \begin{Bmatrix}\sigma_x\\ \sigma_y\\ \sigma_{xy}\end{Bmatrix}^{II} = [\mathbf{T}_\sigma]^{-1}\begin{Bmatrix}\sigma_t\\ \sigma_n\\ \tau_{tn}\end{Bmatrix}^{II} = [\mathbf{M}]_{t-n}{}^{II}\{\boldsymbol{\sigma}\}
\end{aligned} \tag{33}$$

where

$$[\mathbf{M}]_{t-n}{}^{I} = \begin{bmatrix}\underset{3\times3}{\mathbf{M}_0^{I}\mathbf{T}_\sigma^{-1}} & \underset{3\times3}{\mathbf{M}_5^{I}\mathbf{T}_\sigma^{-1}} & \underset{3\times3}{\mathbf{M}_6^{I}\mathbf{T}_\sigma^{-1}} & \underset{3\times4}{0}\end{bmatrix}$$

$$[\mathbf{M}]_{t-n}{}^{II} = \begin{bmatrix}\underset{3\times4}{\mathbf{0}} & \underset{3\times2}{(\mathbf{M}_5^{II}\mathbf{T}_\sigma^{-1})_{2-3}} & \underset{3\times1}{0} & \underset{3\times2}{(\mathbf{M}_6^{II}\mathbf{T}_\sigma^{-1})_{2-3}} & \underset{3\times3}{\mathbf{M}_0^{I}\mathbf{T}_\sigma^{-1}} & \underset{3\times1}{(\mathbf{M}_5^{II}\mathbf{T}_\sigma^{-1})_1} & \underset{3\times1}{(\mathbf{M}_6^{II}\mathbf{T}_\sigma^{-1})_1}\end{bmatrix} \tag{34}$$

$$\{\boldsymbol{\sigma}\} = \left[(\sigma_t)_0^{I}\ (\sigma_n)_0^{I}\ (\tau_{tn})_0^{I}\ (\sigma_t)_5^{I}\ (\sigma_n)_5^{I}\ (\tau_{tn})_5^{I}\ (\sigma_t)_6^{I}\ (\sigma_n)_6^{I}\ (\tau_{tn})_6^{I}\ (\sigma_t)_0^{II}\ (\sigma_n)_0^{II}\ (\tau_{tn})_0^{II}\ (\sigma_t)_5^{II}\ (\sigma_t)_6^{II}\right]$$

$(\mathbf{M}_5^{II}\mathbf{T}_\sigma^{-1})_1$ and $(\mathbf{M}_6^{II}\mathbf{T}_\sigma^{-1})_1$ consist of the first column of $(\mathbf{M}_5^{II}\mathbf{T}_\sigma^{-1})$ and $(\mathbf{M}_6^{II}\mathbf{T}_\sigma^{-1})$. $(\mathbf{M}_5^{II}\mathbf{T}_\sigma^{-1})_{2-3}$ and $(\mathbf{M}_6^{II}\mathbf{T}_\sigma^{-1})_{2-3}$ consist of the second and third columns of $(\mathbf{M}_5^{II}\mathbf{T}_\sigma^{-1})$ and $(\mathbf{M}_6^{II}\mathbf{T}_\sigma^{-1})$.

The formulation of the mixed heterogeneous element guaranteed the stress equilibrium condition along the interface and the displacement compatibility along the interface and element boundary.

Distributed Boundary Stress Conditions

Using the virtual work principle, distributed boundary stress translates to nodal forces. Since the mixed heterogeneous element uses the same displacement functions, the same procedure listed in eqs. (22) can be adopted. Equivalent nodal force resulting from distributed load can be expressed by eqs. (23).

Reissner's Variational Principle

Reissner's Variational Principle enables one to derive

$$\begin{bmatrix} -\mathbf{Q} & \mathbf{C} \\ \mathbf{C}^T & \mathbf{0} \end{bmatrix} \begin{Bmatrix} \boldsymbol{\sigma} \\ \mathbf{V} \end{Bmatrix} = \begin{Bmatrix} \mathbf{0} \\ \mathbf{F} \end{Bmatrix} \tag{35}$$

where $\{\sigma\}$ and $\{V\}$ are expressed in Eqs.(34) and Eqs.(26), $\{\mathbf{F}\}$ is an equivalent nodal force vector applied on displacement $\{\mathbf{V}\}$, and $[\mathbf{Q}]$ and $[\mathbf{C}]$ are

$$\begin{aligned} [\mathbf{Q}] &= t\int_{I}\left([\mathbf{M}]_{t-n}{}^{I}\right)^T[\mathbf{S}^{I}]\left([\mathbf{M}]_{t-n}{}^{I}\right)dA + t\int_{II}\left([\mathbf{M}]_{t-n}{}^{II}\right)^T[\mathbf{S}^{II}]\left([\mathbf{M}]_{t-n}{}^{II}\right)dA \\ [\mathbf{C}] &= t\int_{I}\left([\mathbf{M}]_{t-n}{}^{I}\right)^T[\mathbf{B}^{I}]dA + t\int_{II}\left([\mathbf{M}]_{t-n}{}^{II}\right)^T[\mathbf{B}^{II}]dA \end{aligned} \tag{36}$$

where [S] is the compliance matrix and t is the thickness of materials.

Refer to Eq. (35). Stress vector $\{\boldsymbol{\sigma}\}$ is considered as internal variable vector. It is expressed in terms of the element displacement as:

$$\{\boldsymbol{\sigma}\} = [\mathbf{Q}]^{-1}[\mathbf{C}]\{\mathbf{V}\} \tag{37}$$

Eliminating $\{\sigma\}$ in eq.(35), one can derive

$$[\mathbf{C}]^T[\mathbf{Q}]^{-1}[\mathbf{C}]\{\mathbf{V}\} = \{\mathbf{F}\} \tag{38}$$

<u>Mixed Heterogeneous Elements with Different Interface Locations</u>

Similar to the displacement based heterogeneous element, a total of six mixed heterogeneous elements with different interface locations are developed. They are shown in Figs.18.

IV NUMERICAL EXAMPLES

**4.1 Numerical Example 1**

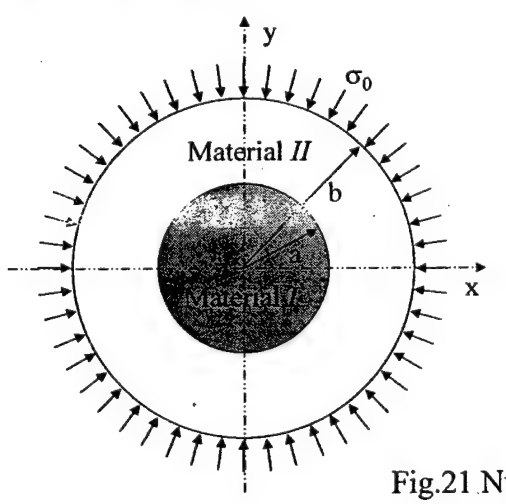


| Material | Young's modulus, $E$ | Poisson's ratio, $\nu$ |
|---|---|---|
| *I* | 200 GPa | 0.2 |
| *II* | 2 GPa | 0.34 |

Fig.21 Numerical Example 1

Fig. 21 illustrates the first example. It consists of two materials. Core material modulus is 100 times ring material modulus. Uniform pressure is applied. A plane-stress state is assumed. Refer to Fig. 21. Assume: $\sigma_0 = 1000$; $a = 1$; $b = 2$.

An analytical solution for this problem exists. Stress distribution in material *I* is:

$$\begin{aligned} \sigma_r^{\ I} &= -\sigma_1 \\ \sigma_\theta^{\ I} &= -\sigma_1 \\ \tau_{r\theta}^{\ I} &= 0 \end{aligned} \tag{39}$$

Stress distribution in material *II* is:

$$\begin{aligned} \sigma_r^{\ II} &= \frac{a^2 b^2 (\sigma_0 - \sigma_1)}{b^2 - a^2} \frac{1}{r^2} + \frac{a^2 \sigma_1 - b^2 \sigma_0}{b^2 - a^2} \\ \sigma_\theta^{\ II} &= -\frac{a^2 b^2 (\sigma_0 - \sigma_1)}{b^2 - a^2} \frac{1}{r^2} + \frac{a^2 \sigma_1 - b^2 \sigma_0}{b^2 - a^2} \\ \tau_{r\theta}^{\ II} &= 0 \end{aligned} \tag{40}$$

where $\sigma_1$ is the radial pressure between the two materials, which is:

$$\sigma_1 = 2b^2 \sigma_0 \left[ \frac{E^{II}}{E^I} (1 - \nu^I)(b^2 - a^2) + b^2 (1 + \nu^{II}) + a^2 (1 - \nu^{II}) \right]^{-1} \tag{41}$$

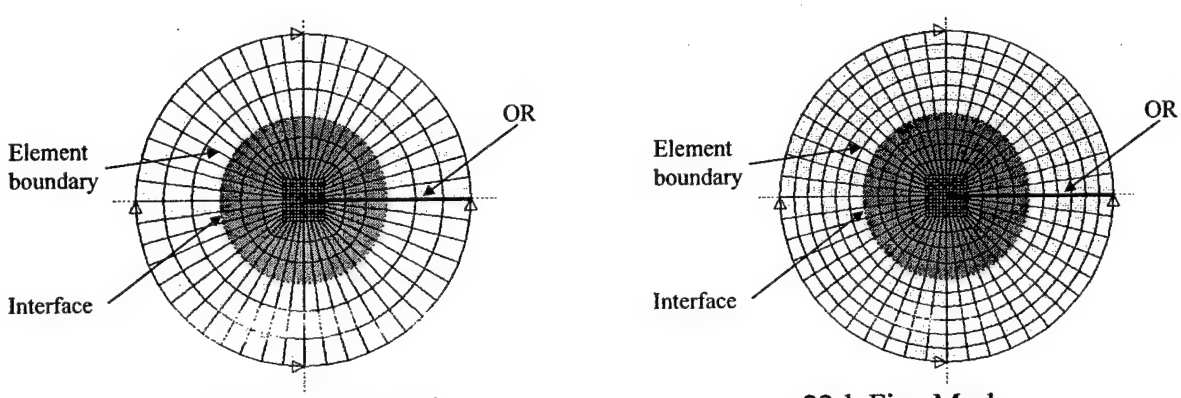


22-a Coarse Mesh

22-b Fine Mesh

Fig.22 Finite Element Mesh

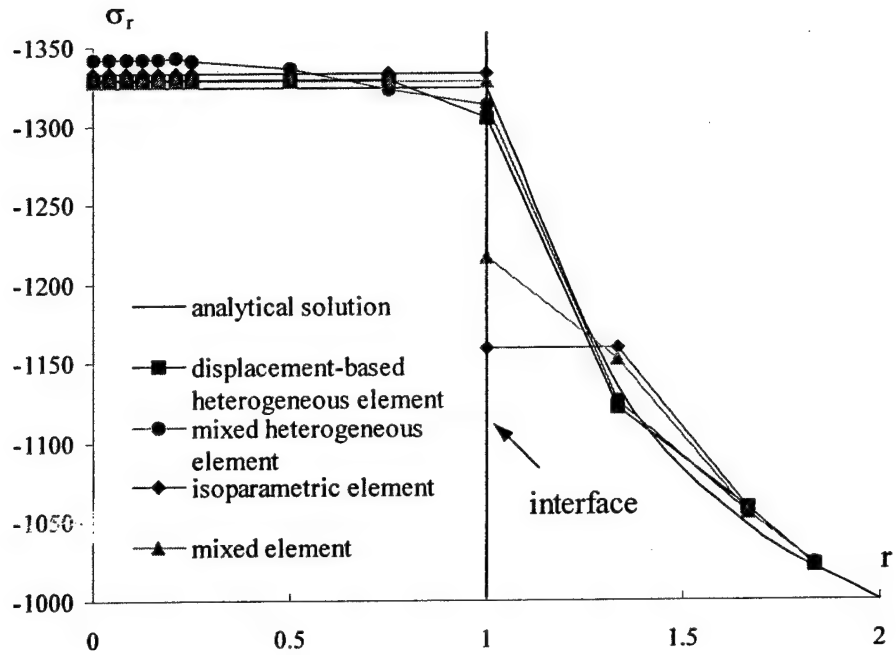


Fig.23-a Comparison of Radial Stress Derived from Four Different Approaches (Coarse Mesh)

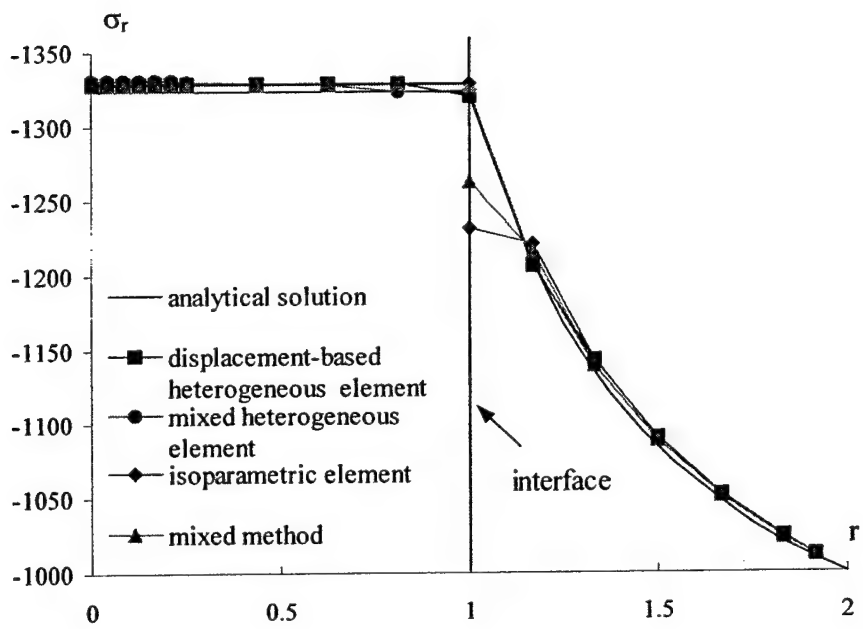


Fig.23-a Comparison of Radial Stress Derived from Four Different Approaches (Fine Mesh)

The two finite element meshes shown in Fig. 22 are used to compare the accuracy of the heterogeneous element approach to conventional iso-parametric (homogeneous) elements and conventional (homogeneous) mixed elements. Fig.23a compares radial stress distribution along the OR (Shown in Fig.22) derived from the coarse mesh. Fig.23b is derived from the fine mesh. Five curves appear in each chart. The black curve is derived from the analytical solution. The red curve is derived from iso-parametric element approach. The green is from the conventional mixed element approach. The blue and purple curves result from the application of the heterogeneous element along the interface. The blue curve is derived from an approach in which displacement based heterogeneous elements are employed along the interface and iso-parametric elements are used elsewhere. The purple curve is derived from an approach in which mixed heterogeneous elements are employed along the interface and conventional mixed elements are employed elsewhere. One finds that the blue and purple curves are very close to the analytical solution. It shows that the application of heterogeneous elements improves accuracy dramatically.

### 4.2 Numerical Example II

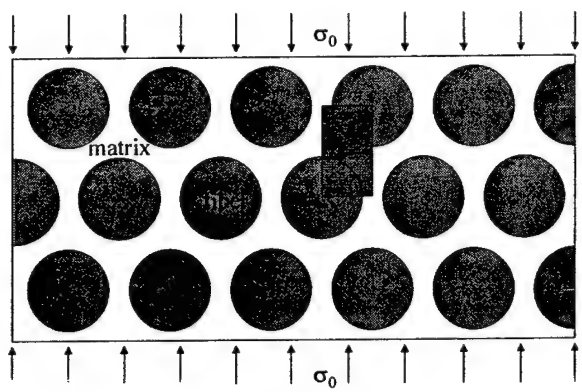


24-a Cross-section

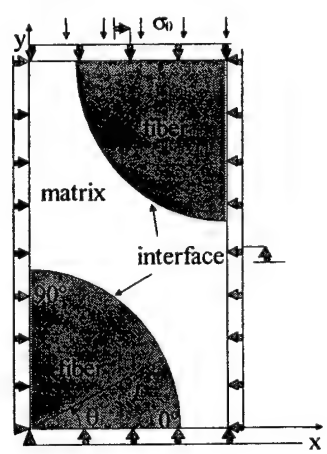


24-b Unit cell and Boundary Conditions
Fig.24 Numerical Example II

Table 1 Material properties of fibers and resin

| Material | Young's modulus (GPa), $E$ | Poisson's ratio, $\nu$ |
|---|---|---|
| Fiber | 325 | 0.15 |
| Matrix | 3.45 | 0.35 |

Figure 24-a shows the material domain of the second numerical example. It illustrates a unidirectional fibrous reinforced composite cross section. Moduli and Poisson ratios of fibers and matrix are listed in Table 1. Because fibers are periodically distributed inside the material domain, only a unit cell is required to determine stress distribution. The unit cell geometry and boundary conditions employed in the numerical analysis are shown in 24-b, which is extracted from the cross-section of 24-a. The plane strain state is assumed.

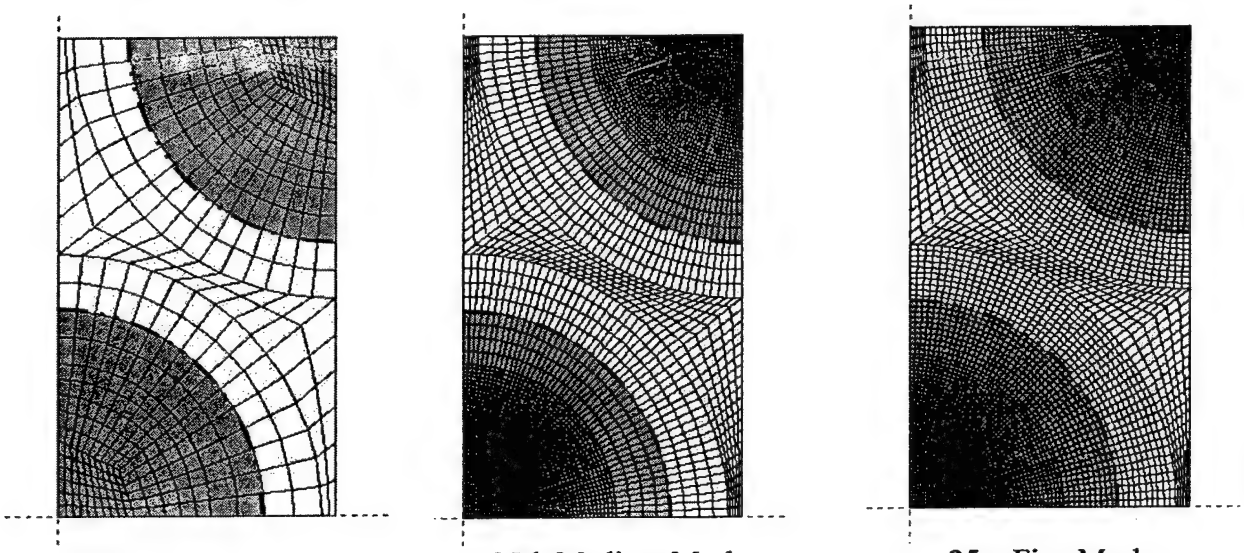

25-a Coarse Mesh 25-b Medium Mesh 25-c Fine Mesh

Fig.25 Finite Element Mesh

Three finite element meshes are used: coarse, medium and fine. Again, the equilibrium along the interface cannot be enforced using either the iso-parametric approach or the conventional mixed element approach. For example, 26-a, 26-b and 26-c shows the interfacial shear stress along the interface derived from conventional iso-parametric and mixed element analysis. One finds that

shear stress derived from the fiber side differs from that derived from the matrix side. The difference becomes smaller with use of a finer element mesh. Theoretically, the difference would approach zero and the stress would approach the actual stress as the size of the element approaches zero. 26-d shows the results with the application of heterogeneous elements along the interface.

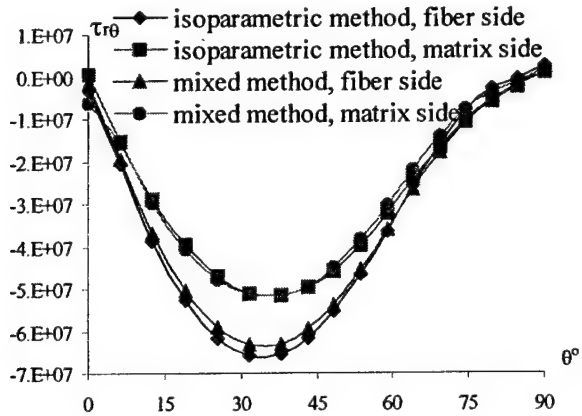


26-a Isoparametric and mixed Element Approach (Coarse Mesh)

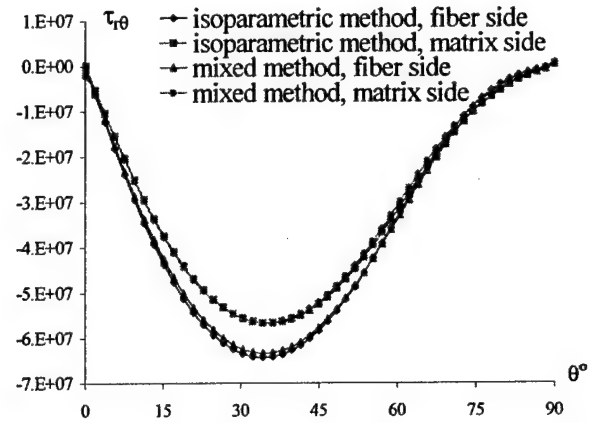


26-b Isoparametric and mixed Element Approach (Medium Mesh)

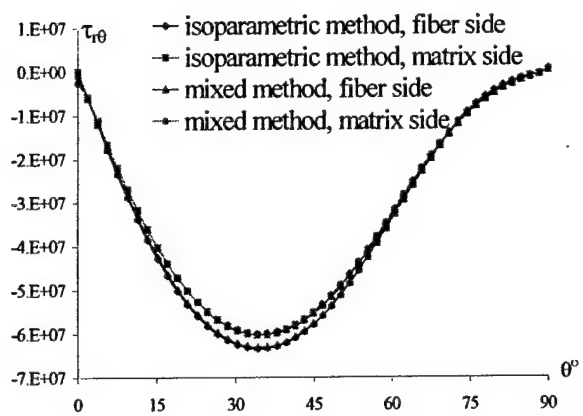


26-c Isoparametric and mixed Element Approach (Fine Mesh)

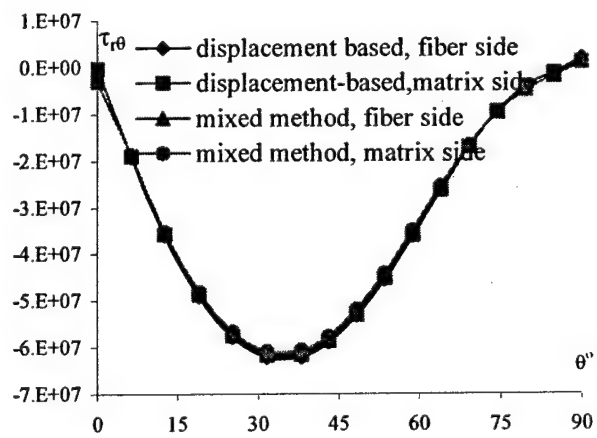


26-d Heterogeneous Element Approach (Coarse Mesh)

Fig.26 Interfacial Shear Stress Derived from Various Element Meshes and Approaches

Fig.27 compares results received from traditional iso-parametric element analysis and results from the application of the displacement based heterogeneous element along the interface. There are six curves in Fig.27. The top two curves are shear stress distribution along the interface at fibers' sides, which are derived from the conventional iso-parametric element approach. The first top one shows the result using the coarse mesh, the second the result using the fine mesh. The bottom two curves are shear stress distribution along the interface of the matrix sides, which are

also derived from the conventional iso-parametric approach. The first bottom one is the result using the coarse mesh; the second the result using the fine mesh. The two curves in the middle are results from the introduction of heterogeneous elements along the interface. Although the coarse mesh is used, the resulting stress curves are located between the two curves derived from the iso-parametric element with the fine mesh. From this one sees the results from use of a coarse mesh in the heterogeneous element is more accurate than use of a fine mesh in an iso-parametric element analysis!

Fig.28 compares results received from conventional mixed element analysis to results from the application of the mixed heterogeneous element along the interface. Six curves are shown. The top two curves show shear stress distribution along the interface at the fibers' sides, which are derived from the conventional mixed element approach. The first top one is the result using the coarse mesh; the second the result using the fine mesh. The bottom two curves are shear stress distribution along the interface at the matrix sides, which are also derived from the conventional mixed approach. The first bottom one is the result using the coarse mesh; the second the result using the fine mesh. The two curves in the middle are results from the introduction of heterogeneous elements along the interface. Although the coarse mesh is used, the resulting stress-curves are located between the two curves derived from the iso-parametric element with fine mesh. Again, from this, one sees the results from use of a coarse mesh in the heterogeneous element is more accurate than use of a fine mesh in an iso-parametric element analysis!

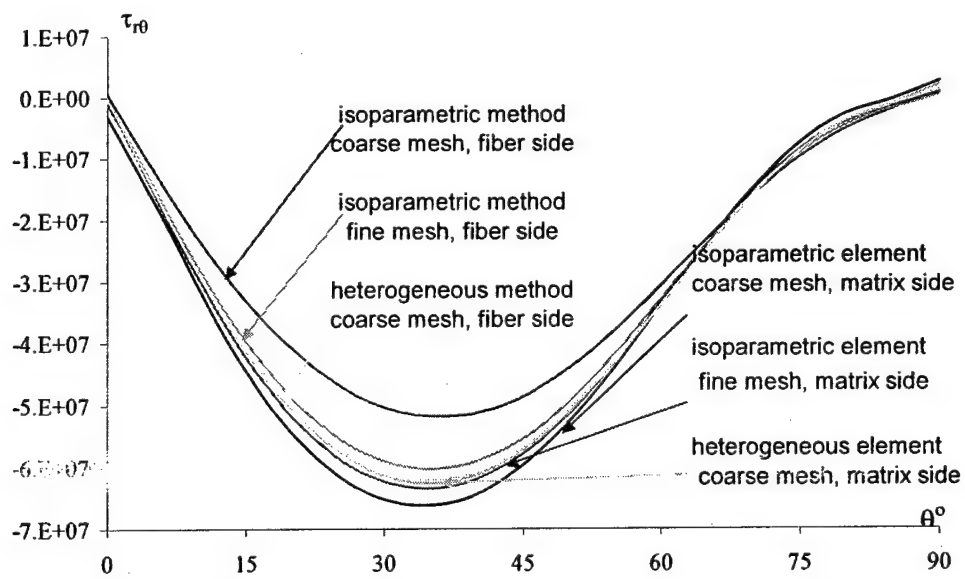


Fig.27 Comparison of Shear Stress along the Interface Derived From Displacement Based Heterogeneous Element Approach and Iso-parametric Element Approach

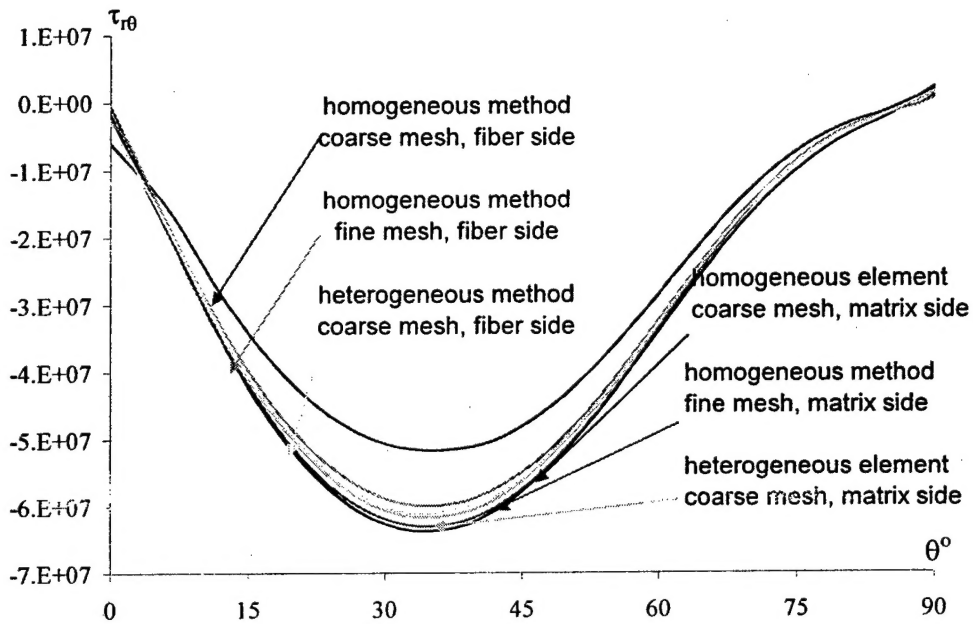


Fig.28 Comparison of Shear Stress along the Interface Derived From Mixed Heterogeneous Element Approach and Conventional Mixed Element Approach

### 3.4.3.Simplified Mesh Generation

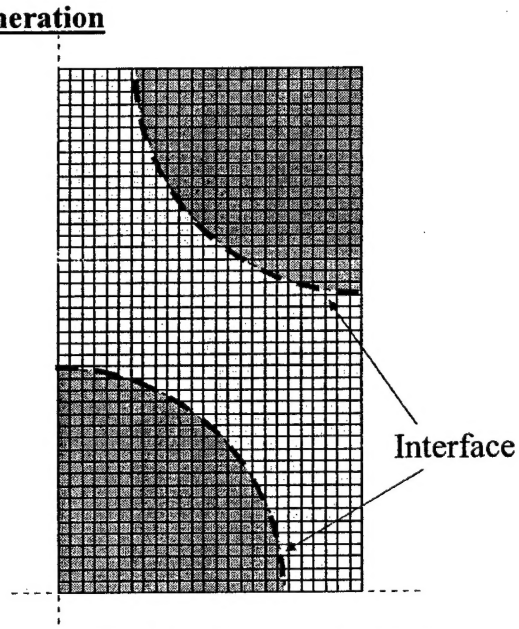


Fig.29 Rectangular Mesh

As aforementioned, one difficulty with use of finite element analysis for composites is the time-consuming mesh generation process. The heterogeneous element can contain more than one material. There is no need to match the element boundary to the interface. Simplified mesh

generation, therefore, can be used. For example, the unit cell used in the previous sub-section can be descretized into a rectangular element mesh as shown in Fig.29. The dotted red curve represents the interface. Elements along the interface are heterogeneous. Other employed elements are conventional iso-parametric. Fig.30 shows the calculated interfacial normal and shear stress distributions using both simplified rectangular mesh and the previous mesh. Again, results derived from the previous mesh and from the rectangular mesh are very close.

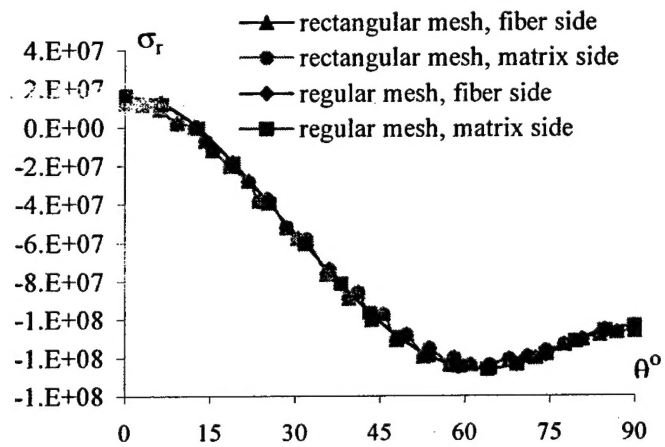


30-a Radial Stress along the Interface

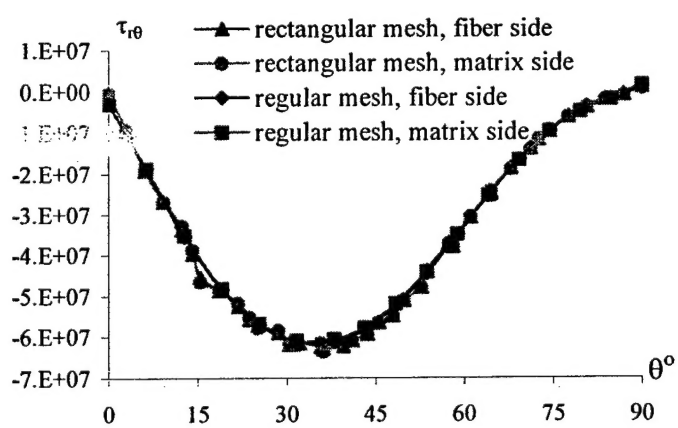


30-b Shear Stress along the Interface

Fig.30 Comparison of Interfacial Stress Derived Using Rectangular Mesh and Regular Meshes

## 3.4 Summary on Heterogeneous Elements

Two Heterogeneous element formulations are developed: displacement based and mixed. In the former formulation, displacement compatibility is enforced along the interface between two

dissimilar materials, along the boundary between heterogeneous elements, and along the boundary between heterogeneous elements and iso-parametric elements. The equilibrium condition is satisfied in a weak form. In the latter formulation, not only is the compatibility along the interface of dissimilar materials on the boundary between heterogeneous elements and conventional mixed elements enforced, but the equilibrium condition is also strictly enforced.

Numerical results show that replacing a homogeneous element at the interface area with a heterogeneous element improves accuracy significantly. In addition, the mesh generation process is immensely simplified. Because one heterogeneous element can contain two materials, there is no need to match the element boundary with the interface. A simple rectangular mesh can be adopted.

## IV. IMPACT OF THE PROJECT

The "Digital element approach" is a unique technology for textile mechanics that has been developed through the research project. It is the only model that can analyze textile fabric deformation based upon fiber-scale mechanics. It can be used for textile process design of composite structural components, for deformation simulation of textile fabrics during the molding process and for the prediction of textile preform micro-geometry, such as yarn paths, yarn cross-section deformation and fiber paths. Further, it can be used for dynamic analysis of textile fabrics, such as for the high penetration failure mechanism of textile fabrics and for textile micro-/nano- device design.

The "Heterogeneous element approach" is a new element method developed through the research project specifically for composite materials. The concept is that an element can consist of more than one material. The formulation of the heterogeneous element enforces both the stress equilibrium conditions and displacement continuity at the interface between fiber and matrix. As a result, the convergence rate of the heterogeneous element approach is much faster than the conventional iso-parametric element approach. Two kinds of heterogeneous element formulations have been developed: A displacement based heterogeneous element and a mixed heterogeneous element. Preliminary tests show that 80-90% less elements are required in the vicinity of the interface if the heterogeneous element approach is employed.

## V. PERSONNEL SUPPORTED/ASSOCIATED:

| | |
|---|---|
| Principal Investigator: | Youqi Wang (Associate Professor) |
| Assistant Research scientist: | Eric Zhou |
| Post Doctorate Associate: | Xuekun Sun |
| Ph.D. Graduate student: | Chen Tao |
| Master graduate student: | Jason Rahn |

## V. PUBLICATIONS

1. Guangming Zhou, Xuekun Sun and Youqi Wang, "Multichain digital element analysis in textile mechanics," Composites Science and Technology, 2003.

2. Chen Tao, "Heterogeneous Element: A New Finite element Method for the Micro-Stress Analysis of Composites," Ph.D. Thesis, Kansas State University, 2003.
3. Youqi Wang, Changjie Sun and Xunkun Sun, Nicholas J. Pagano " Principles for recovering micro-stress in multi-level analysis," ASTM STP 1416, Composite Materials: Testing, Design, and Acceptance Criteria, A.Zereick and A.T. Nettles, Eds., American Society for Testing and Materials International, 2002.
4. Youqi Wang, Xuekun Sun and Guangming Zhou, "Application of Digital Element in Textile Mechanics," TEXCOMP-6, Philadelphia, 2002.
5. Youqi Wang and Chen Tao, "Analysis of fiber-matrix interfacial stress analysis by using heterogeneous finite element," ICCM-12, Paris, July 1999.
6. Youqi Wang and Xuekun Sun, " Digital element simulation of textile processes," Composites Science and Technology, 61(2):2001.
7. Youqi Wang and Xueknu Sun, " Determining the geometry of textile preforms using finite element analysis," 15th Technical Conference of American Society for Composites, Taxes A&M, Sept. 2000.
8. Xuekun Sun and Youqi Wang, "Geometry of 3-D braided rectangular preform with axial yarns," SAMPE 2001, May, 2001.
9. Changjie Sun and Youqi Wang, "Determine the size of "local domain" in multi-scale analysis," ICCM 13, Beijing, June, 2001.

## VI. NEW DISCOVERIES, INVENTIONS, OR PATENT DISCLOSES:

Two numerical methods are developed:

1. Digital element simulation approach
2. Heterogeneous finite element method